Heritage Science

RESEARCH

Open Access

From RGB camera to hyperspectral imaging: a breakthrough in Neolithic rock painting analysis

Bernard Schmitt[1*], Zahira Souidi[2], Frédérique Duquesnoy[3] and Frédéric-Victor Donzé[4]

Abstract

Rock paintings undergo physical, chemical, biological and/or anthropic alterations that alter their visibility. Cameras and image enhancement tools (DStretch® plug-in, for example) are commonly used to help identify and record images that have become invisible to the naked eye. HyperSpectral Imaging (HSI) which is strongly developing in many research and application fields, is tested in this study to analyze Neolithic rock paintings. We particularly address the question of what kind of additional information can Visible Near InfraRed HSI instruments, coupled to mathematical transformations to reduce the dimensionality of the data, bring for rock paintings, compared to standard RGB cameras. From the analysis of a selection of panels painted on yellow-reddish altered sandstone walls and measured in Saharan shaded shelters, we show that HSI can reveal new figures by capitalizing both on its ability to extract the different pigment types with a greater contrast, and on the new discriminating information contained in the very near infrared part of the spectrum. Despite their much smaller image format, HSI can provide up to 5–7 contrasted images of the spatial distribution of the different types of pigments in the figures. It thus appears to be a promising non-invasive and efficient methodology to both reveal disappeared paintings and to study image juxtapositions and painted layer superimpositions.

Keywords Rock paintings, Archeology, Neolithic, DStretch®, HyperSpectral Imaging

Introduction

Compared to techniques like freehand drawing, direct tracing or silver photography, digital photography and image enhancement software have dramatically improved the processes of documenting and studying rock art paintings [1–5]. Bringing more accurate and objective surveys [6, 7], these techniques not only facilitate the study of visible paintings [8–10], but also make it possible to discover new ones, either previous paintings, underdrawings or *pentimenti*, that we did not even know existed [11].

Digital photography has also proven particularly suitable for remote fieldwork due to its ease of use. Yet, to document rock images, it requires a camera with a sufficient resolution, a skilled operator to control the various parameters during the shooting, as well as advanced post-processing of the shots. Nevertheless, it is possible to make usable pictures without being an expert, as long as the shooting conditions are not extreme. The contribution of image processing software to the study of rock art images has mainly concerned the enhancement of pictures, in order to reveal what the human eye could perceive with difficulty on site. These post-processing stages were developed in the beginning of the 1980s, when an image was scanned before being processed on a

*Correspondence:
Bernard Schmitt
bernard.schmitt@univ-grenoble-alpes.fr
[1] Université Grenoble Alpes, CNRS, IPAG, 38000 Grenoble, France
[2] Université de Ain Témouchent, Belhadj Bouchaib, Algeria
[3] Université Savoie Mont Blanc, CNRS, IRD, IFSTTAR, EDYTEM, 73370 Le Bourget-du-Lac, France
[4] Université Grenoble Alpes, Université Savoie Mont Blanc, CNRS, IRD, IFSTTAR, ISTerre, 38000 Grenoble, France

computer. Mickael R. Rip [12, 13] was one of the first to assess this methodology on a rock-painting picture.

From then on, image enhancement software diversified as their performance increased, together with the arrival of digital cameras [14–17]. In addition, image enhancement has also proven to be effective in monitoring the evolution in terms of degradation of the paintings as well as localized areas of the supports. This use for conservation purposes is currently an application under development [10, 18, 19].

Among the software currently used for rock arts, the "standard" is Photoshop©, produced by the company Adobe© [2, 3, 20–22]. Another software appears to be particularly well adapted to the study of rock paintings, because of its processing speed, very low cost and ease to use: DStretch®, a free plugin for ImageJ©, specifically designed in 2005 by Jon Harman [21, 23]. Ever since it became available [3], DStretch® has been widely used over the last 15 years by many rock art archaeologists [5, 24–27] as well as by Learned Societies like the AARS (Association of the Friends of Saharan Rock Art) [28]. To enhance digital photographs of cave paintings, DStretch® uses a decorrelation algorithm originally developed in 1978 at the Jet Propulsion Laboratory in Pasadena, California, where it was used to improve the contrast of Landsat multispectral images [29]. It was then used with the ASTER (Advanced Spaceborne Thermal Emission and Reflectance Radiometer [30]). In 2004, NASA released images from the Rover mission to Mars, which had been enhanced with this technique and which suggested that it could also work well on photographs of cave paintings.

DStretch® has been developed to process Red–Green–Blue (RGB) camera pictures only. Since only three visible bands are available, its ability to separate and enhance different information is limited. Most standard cameras work with RGB bandpass filters in a Bayer mosaic covering the 400–410 to 670–690 nm range (at 2% Green maximum, [31]), i.e. about the human eye photopic sensitivity range (~ 420–675 nm at 2% of eye sensitivity maximum, [32]) which is limited to a very small portion of the whole electromagnetic spectrum. This feature presents a severe limitation when attempting to detect remaining painting pigments invisible to the naked eyes. Hyperspectral imaging (HSI) technology may be used for this challenging application by recording hundreds of bands across a wider spectral range (see e.g. [33]). Those bands are contiguous, narrow and regularly sampled and are not limited to the visible part of the spectrum. HSI provides a well sampled spectral signature at each pixel of the image creating a three-dimensional data cube or hypercube. A frame hypercube is composed by a sequence of images each corresponding to individual spectral bands acquired by the camera (Fig. 1).

After several generations of multispectral imagers (with only a few wide and specific spectral filters), HSI has been

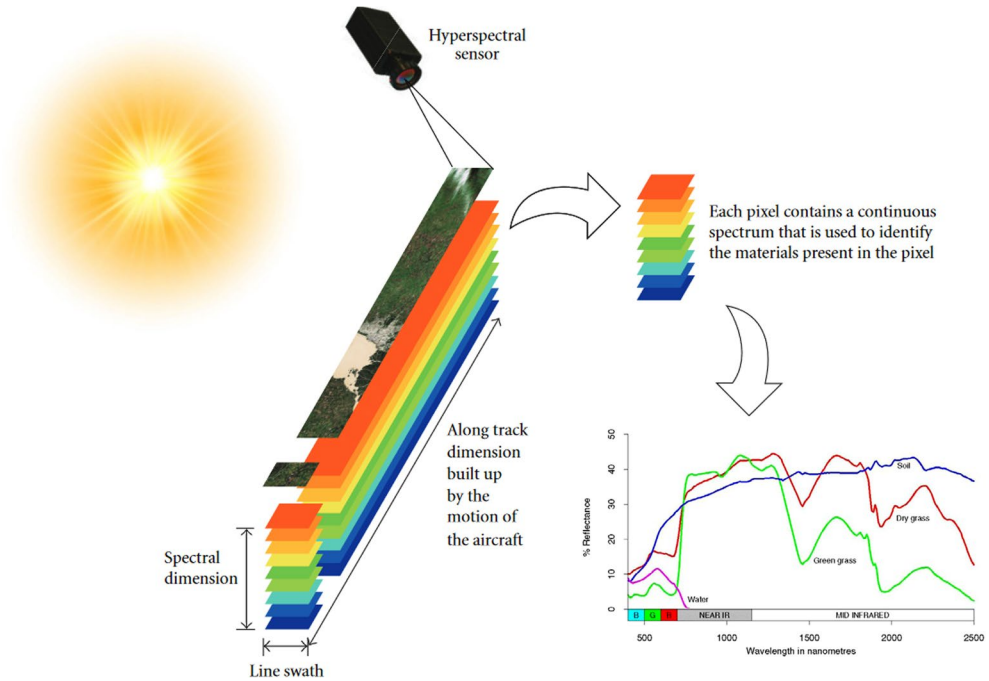

Fig. 1 In a hyperspectral imaging's pushbroom mode, the camera scans the surface line by line and record a full spectrum at each pixel location. An image at each wavelength forming a 3D data cube is obtained (Two spatial dimensions and one in the spectral dimension) (adapted from [34])

developed for space exploration missions since the late 1980s (French ISM instrument on the Phobos missions, [35]) and on aircraft since the 1990s and then on Earth's observation satellites since the late 2000s [36]. Presently, hyperspectral cameras are used indoor (laboratory, industry…), in the field and now often mounted on UAV platforms. They can be classified according to the methodology by which these sensors build the hypercube. A pushbroom (or line scan) sensor records images line by line in motion (Fig. 1), while spectral scan instruments record single images for each spectral band selected sequentially in time, and snapshot hyperspectral imagers record the image at all wavelengths at the same time. For about two decades HSI have been more and more widely used for various application including geology [33, 37], industry, environment, agriculture [33], agri-food, forensic [38], biotechnologies and medical diagnosis [39], as well as art painting where it is becoming an essential tool for the historical study of the technical realization of the paint layers and underlying material of the artwork [40–44], their restoration [45, 46], as well as for their expertise [47]. The HSI technique strongly improves the collected information in the spectral dimension (to the detriment of spatial resolution) and complements the pioneering studies using multispectral imaging and pulse-compression thermography at high spatial resolution, developed in particular in the field of art work studies [48, 49].

Each painting pigment has its unique composition and texture and therefore reflects sunlight according to its characteristic spectral signature over the electromagnetic spectrum (see e.g. [50]). However, rock paintings undergo physical, chemical, biological and/or anthropic alterations that alter their visibility, i.e. its contrast relative to the underlying rock. Nevertheless, we can expect that its distinctive spectral pattern, fully sampled by an HSI, is still recognizable at least in some spectral ranges and may detect the presence of tiny amounts of pigment. Because of both the increased spectral range and the number of measurement channels, HSI can provide a larger amount of information that may allow us to identify the screened materials, and separate them from the underlying rock, based on their chemical composition rather than only their remaining perceived visible colors. As an example, the spectrum of a very thin layer of red pigment painted on a flat slice of brown carbonate rock compared to the VNIR spectrum (Visible-very Near InfraRed: 400–1000 nm) of the rock itself [50] is shown in Fig. 2. The spectral signals present clear spectral and photometric differences between the painted and the non-painted zones, in particular above 650 nm, while the simulations of the RGB signal of a classical digital camera (Canon 20D) present only a very small difference in hue (~ 6%) and radiometric brightness (average ~ 10%). Such a difference may be not significant enough on a more inhomogeneous rock wall because spatial variations of rock texture and composition, or the lightning nature and orientation can also produce it. It should be

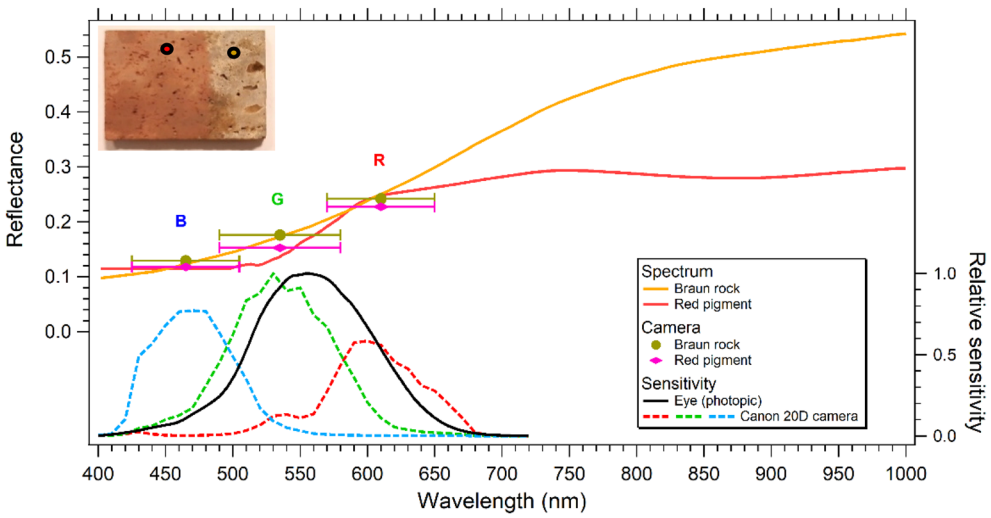

Fig. 2 Comparison between spectra of VNIR hyperspectral imaging and signal of classical RGB camera for typical rock painting pigments. The high-resolution reflectance spectra measured on a very thin layer of red 'Beauregard' pigment (red) painted on a carbonate rock, and the non-painted rock itself (brown) are plotted with a continuous line (left scale) [50]. The large dots are simulations corresponding to the RGB signal of a digital camera (Canon 20D, [31]) extracted from these spectra by convolving them with its filter band passes (dotted lines at the bottom, right scale) with 'error bars' representing the full width at half maximum of the three filters. The bottom black curve is the total photopic eye sensitivity [26]

noted that the perceived brightness difference between the paint and the substrate in Fig. 2 is larger (~25%) because the photopic eye sensitivity is peaking near the green where the brightness difference is the largest, in that specific case.

The numerous spectral channels of an HSI camera should also provide a better discrimination between the various pigment materials used in a polychromic painting, even between paints of very similar colors in a 3-channels RGB image [41, 45, 46]. Finally, we can also expect detection of underlying paintings due to the large transparency windows of numerous mineral pigments in the very near (700–1000 nm) and short-wave infrared ranges (SWIR: 1000–2500 nm). The use of these infrared wavelength ranges for revealing underdrawings and *pentimenti* are already well established for art work inspection [48].

Until now, studies of cave art have used RGB cameras and image enhancement tools (DStretch® plug-in for example) to help identify images that have sometimes become invisible to the naked eye and to make a survey [24, 25, 27]. Multispectral imagery, mostly by adding channels in the Near-IR [42], or using true multispectral instruments [51] have shown the advantage to extend the wavelength range outside the visible spectrum to study artwork. This technique has been discussed since a long time for rock painting [52] but only tested up to now [53–57]. In particular, Bayarri in his PhD, appears to have performed 5-band multispectral measurements in both the Near-IR (<2500 nm) and mid-IR (>2500 nm) ranges [56].

To our knowledge, only one group has done pioneering work with VNIR hyperspectral imaging, to study prehistoric rock painting in two Spanish caves [56–60]. They used four sets of three lamps for the illumination of the panels. From their analysis of some panels painted on the limestone wall of the cave of El Castillo (Spain) they were able to identify 76% more figures, some of them below a calcite layer, and to differentiate between slightly different paints. They concluded that hyperspectral imaging could become an efficient tool for the recognition of figures, coloring matter and state of conservation.

The objective of this study is to show what kind of useful additional information VNIR HSI imaging can bring in the case of rock painting on yellow-reddish oxidized sandstone walls measured in shaded shelters, compared to standard RGB cameras. In particular we are focusing on the capacity of HSI to detect invisible/barely visible figures, to extract the pigment distribution from the rock texture pattern and to separate the different paint layers. 'Visual simulations' using only the visible range of the HSI data is out of the scope of this paper. The images we provide are B&W or 'false color' synthetic images to best display to the eye the 'invisible' and mathematically transformed spectral information contained in HSI data.

As an application case a lightweight portable VNIR HSI camera has been used in the Sahara, i.e. in a particular rough field, to take pictures of large painted surfaces using an HSI without special lighting, just as would be done with a regular camera. The aim was to allow a quick and easy implementation for extensive non-contact imaging measurements and thus the possibility of exploring hard-to-reach areas. This paper presents the measurements and the analysis of a selection of painted panels of increasing complexity and will draw conclusions from a remote sensing point of view on the detectivity, separability and extraction of pigments, but will not address any archeological consideration or artistic interpretation of the highlighted figures.

Materials and methods

Studied rock painting panels

The panels used for these tests are located in central Sahara. If many of them are well-preserved, many more are very faded (Fig. 3a) because they were painted on the walls of open rock shelters (Fig. 3b). Among factors that may affect the conservation state of those paintings are the low rainfall and the rising temperatures [61, 62] which appear to have increased in recent decades. This accelerated climatic deterioration could have a double effect: on the one hand, to accentuate the process of

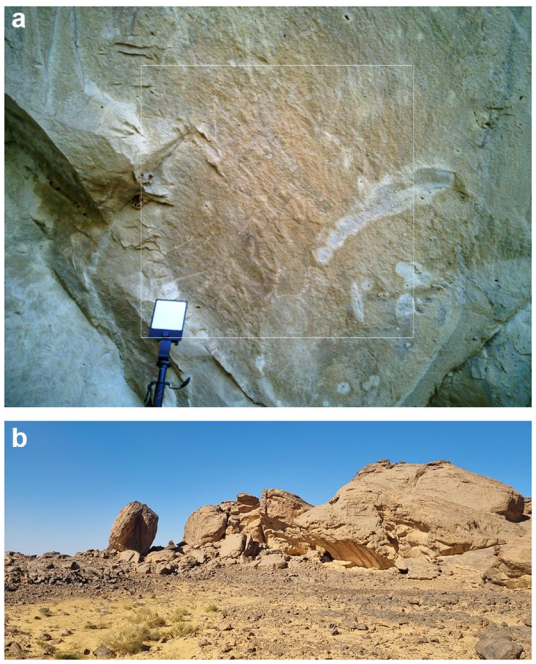

Fig. 3 An example of a faded rock paintings which is analyzed in this study (**a**). View of a typical rock shelter (**b**)

flaking of the walls used as support to the paintings, by a phenomenon of desiccation, and on the other hand, by increasing the intensity of the abrasion related to the corrasion, i.e. erosion by the action of sand grains carried by winds on the most exposed walls [19]. Additional degradations in some areas come from modern tagging over the painted figures.

Data acquisition using classical RGB camera

Highly portable RGB cameras were used to meet the difficult field conditions and among them, a Samsung galaxy S21 integrated camera. This camera has three multi-rear cameras with several functions. We used the 64 Mpx f/2.0 telephoto camera with 1.1 × optical zoom to take pictures of rock paintings (Fig. 21a).

DStretch® process from classical RGB camera

Different types of stretching algorithms (decorrelation stretch (DS), photographic stretch, saturation stretch, …) and transformation algorithms (PCA, ICA, MNF) may be applied to RGB images to enhance the information it contains. Some comparisons have been already made between DS and PCA, showing that the later was slightly more efficient [63]. We made some tests of all these algorithms on several of the images presented below and finally decided to use only decorrelation stretch throughout this study by using the DStretch® software, the only algorithm/software widely used as a reference tool by prehistoric archaeologists. Thanks to its flexibility in use and its optimization to the specific problem of rock painting it provides among the best results when faint paints are present. In some cases, ICA or MNF transformations gave slightly better results in terms of figure contrast or paint-rock separation than DStretch® but in none case they allowed to detect the invisible figures highlighted by the analysis of the HSI data presented in Sect. "Results".

Dstretch enhances the color separation in images with high interchannel correlation. If one views the pixels from 3 channels of a RGB photo as 3-vectors, this is done by first finding the linear transformation that results in removing the correlation among the vectors in the transformed space. This is an eigenvector problem, and can be considered of as a rotation of the coordinate system of the original vector space. Within this rotated space, each component is rescaled (i.e. contrast stretched) by normalizing the variances of the vectors. Then the rotation that returns the vectors to the original coordinate system is applied. Both of the rotations and the variance normalization step can be described by matrix and vector operations, and can be combined into a single mathematical operation that operates on the input photo and produces the decorrelation stretched output. The result of the process is an output image whose pixels are well distributed among all possible colors, while preserving the relative sense of hue, saturation, and intensity of the input image [30].

With most image enhancement software, the result is very much related to the level of expertise of the operator. It can therefore be extremely variable, whereas with DStretch® it depends much less on the operator, at least at the first level of use, which is largely sufficient in most cases. This allows for more objective and easily reproducible results, which is essential for an accurate study of the art [10, 17]. These twenty-three color spaces are currently defined as standards while processing rock paintings with DStretch®. However, image enhancement has the built-in limitation of the three RGB measurement channels, and thus strongly depends on the intensity and visual color of the paint.

Data aquisition using HSI Specim IQ camera

Field captures of rock paintings were performed with a SPECIM IQ (Fig. 4), an HSI system operating in the VNIR, which is based on an internal line scanner process, i.e., push broom principle. It covers the whole wavelength range 400–1000 nm at a spectral resolution of 7 nm. Its characteristics are summarized in Table 1 [64]. A 1.2 Megapixels RGB context image with slightly better resolution fully including the HSI field of view is also recorded simultaneously with the 'viewfinder' camera. This context image is taken from virtually the same point of view (2.5 cm above the HSI lens) and with exactly the same illumination. It will be used, raw and processed with DStretch©, to compare with the HSI results.

Table 1 Characteristics of the SPECIM IQ hyperspectral imaging system and its context RGB camera [64]

Hyperspectral imager	**SPECIM IQ**
Sensor type	CMOS
Spectral range	400–1000 nm
Spectral resolution	7 nm
Spectral bands	204
Image size	512 × 512 px
Focal length	21 mm
Field of view (fixed lens)	31 × 31°
Imaged wall @ 1 m	55 × 55 cm
Spatial resolution @ 1 m	1.07 mm
Focus range	15 cm–infinity
Weight	1.3 kg
Context RGB image	
Image size	1280 × 960 px
Imaged wall @ 1 m	110 × 82 cm
Spatial resolution @ 1 m	0.85 mm

Fig. 4 The Specim IQ camera in the field measuring rock paintings

As common for any hyperspectral measurement, a suitable lighting providing a continuous spectrum over the wavelength range of interest is required. In our case, to avoid the complex and power consuming use of artificial lighting in the field, our illumination source was mostly sunlight scattered by the perfectly clear sky and the surrounding landscape since rock paintings are located on shelters' walls. The sky contribution (more than 60% of the solid angle) provides a bluer light with strongly decreasing intensity in the very near infrared (40 times less Rayleigh scattered light at 1000 nm than at 400 nm) compared to the sun spectrum which, combined with the decrease of sensitivity above 700 nm of the CMOS detector, limits the useful spectral range below 920 nm. The spatial variation in intensity across the measured area remains limited (a maximum of a few percent estimated in a particular case from measurements of the Spectralon® panel at different places in the field of view) and very smooth because of the diffuse multidirectional illumination and the small and relatively flat measurement area (typically 50 × 50 cm) compared to the size of the rock wall of the shelters (several meters). The spectral variation of the illumination is also faint and smooth across the image. The temporal variation during the frame acquisition (< 2 min) is also negligible as the weather was always offering a perfectly clear sky.

Here after, we present some key information to reproduce our technical approach. The measurement process includes seven steps:

1. Reference panel: after selecting the field of view of the HSI camera, a white reference panel (Spectralon® 99%, 10 × 10 cm) is positioned next to the painted wall in the field of view of the instrument to allow to capture the spectral characteristics of the wall lighting at the same time as the image (simultaneous white reference).
2. Focusing: the hyperspectral camera is then focused on the target using the viewfinder camera, i.e., a small RGB camera situated just above the spectral camera, with identical viewing direction but larger field of view. The focusing is done manually by highlighting sharp edges.
3. Context image: to overlay the spectral and viewfinder camera images their parallax is corrected either automatically or manually.
4. Integration time: then, the integration time is adjusted (in the range 1–500 ms). The viewfinder camera image provides an evaluation for the integration time of the spectral camera but a manual optimization was always made in order to use 80–90% of the capacity of the detector while being cautious about saturation, especially in the white reference target.
5. Recording: after these initial adjustment steps, the image recording process is triggered. At first, a dark reference image representing the sensor background noise and read noise, without incoming light is recorded automatically. Then, the line scanner starts the actual data acquisition.
6. Validation and reference selection: after the full 512 × 512 pixels image is scanned, the focus and possible saturation or under-exposition are checked in the data validation view with a synthetic RGB image derived from the hyperspectral image cube and minimum and maximum intensity pixel histograms. If the image is validated, part of the white area of the Spectralon® reference target (typically 2000–8000 pixels depending on camera-wall distance) is then selected by thresholding the intensity of the image followed by a pixel connectivity algorithm.
7. Calibration: after removal of the dark background the calibration process converts the image cube in 'reflectance factor' unit by dividing the spectra of all pixels by an average spectrum of the selected area of the Spectralon® reference. All the data are automatically stored, the raw and calibrated hyperspectral data cubes, the dark and white reference spectra, an RGB preview of the HSI data and the RGB context image.

Hyperspectral data analysis

A set of hyperspectral reflectance data obtained on various sites have been analyzed using different standard tools available in the standard ENVI® hyperspectral image software (Version 5.5, L3HARRIS GEOSPATIAL™). The results have been compared to

the simultaneously recorded context RGB image (with only 20% better spatial resolution, but identical lighting and viewing geometry) as well with very high-resolution images of the same scenes recorded by the different cameras (listed in 2.2) and analyzed with DStretch®.

Several unsupervised mathematical transformations aimed at extracting and packing the information contained in hyperspectral image cubes have been tested and compared:

- Principal Components Analysis (PCA), with covariance matrix.
- Independent Components Analysis (ICA), with Log-Cosh contrast function and 2D spatial coherence sorting.
- Minimum Noise Fraction Transform, (MNF), with noise statistics from whole image.

They are called 'rotations' as they aim at changing the base on which the dataset is projected in order to reduce the dimensionality of the useful data (initially 204 spectral information planes, one at each wavelength) and to segregate the noise in the data. Their working hypotheses on the initial content of the data are however different and the recently developed ICA [65] is expected to be the most efficient transformation to separate different layers of information, i.e. different types of paintings as well as rock composition and texture. This transformation is generally used for 'blind source separation', with no a-priori information on the mixing. It assumes non-Gaussian distribution of the independent information sources, which is typical of natural hyperspectral datasets, and uses high-order statistics to reveal interesting but faint features or covering only a small portion of the image.

These transformations are frequently used in space exploration and remote sensing data analysis [e.g. 65] and more recently PCA was introduced and commonly used in art work studies [42, 43, 63]. In rock art PCA was used for analysis of camera images [52, 63, 67] and one group [56, 57, 60, 68] used all these algorithms in parallel on hyperspectral data to analyze rock paintings but did not discussed their relative advantages. However, Cerrillo-Cuenca et al. [69] very recently made a thorough comparison of PCA and ICA on camera images of superimposed rock paintings. They concluded that "*ICA accurately separates panels with more than one type of colour, while PCA achieves a lower degree of separation*". They also showed that "*in scenes with monochrome depictions, ICA tends to be slightly more effective in separating the pigments from the rock*."

But before running the transformation, several preliminary analyses of the data cube and a few conversions are necessary in order to optimize their results. First the data cube needs to be rotated 90° clockwise to go back to the original vertical view. Then the reference target and its shadow, which may adversely alter the image statistics of the rock painting due to their extreme and constant brightness values, needs to be removed by applying a spatial mask to the image. Finally, from local statistics on the very homogeneous spectra of the reference target (Fig. 5) coupled with an analysis of a selection of individual spectra (Fig. 10), we can select the spectral range

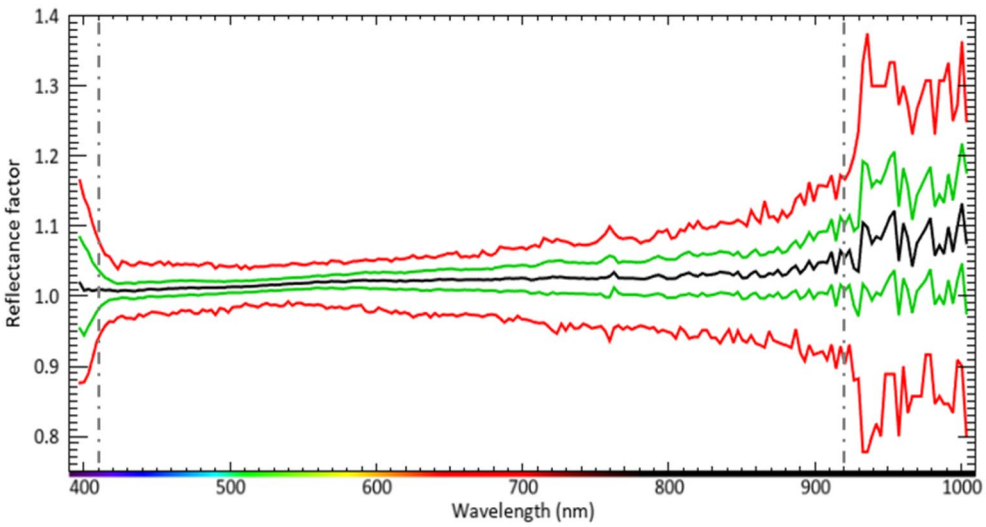

Fig. 5 Statistics on the spectra of the reference target (~ 2700 pixels) with mean (black), mean ± standard deviation (green), min and max values (red) showing the increasing noise below 410 nm and above 920 nm. Only the central part of the spectrum (dashed lines: 410–920 nm) with standard deviation < 5% is kept for the hyperspectral data analysis

in which the signal-to-noise ratio is large enough while keeping enough channels to preserve most of the useful information and to run efficiently the ICA transformation. Removing the noisiest channels should improves the detectivity of subtle painting that otherwise may remain buried in noise. The first five spectral channels in the deep blue (< 410 nm) and the 923–1000 nm very near infrared range receive very little light and are removed from this analysis. The hyperspectral data cube is thus restricted to the 410–920 nm range, i.e. 172 spectral channels (instead of 204). Tests on a few data sets showed that both these spectral and spatial filtering, commonly used in the analysis of space exploration hyperspectral images [65], significantly improved the quality of the results in particular in terms of noise segregation.

Figure 6 presents the comparison between the different synthetic results obtained from the PCA, ICA and MNF mathematical transformations for one of our case studies (panel #2, see part "Panel #2: separation between a complex wall and pigments"). The different transformations applied on the HSI data, because of the numerous spectral channels and extended range, not only efficiently separates the large-scale effects of the rock texture from the painting patterns but also removes a large fraction of the 'noise' in the components containing the pigment and rock information. This 'noise' might be a purely instrumental noise but it can be also high spatial frequency fluctuations of the reflected signal due to the microscopic texture of the rock inducing random local illumination and reflection angles, micro-shadows as well as color variations at the pixel scale.

From a detailed comparison between the results of ICA and the other transformations, it appears that the PCA and MNF transformations are not able to separate as well the different painting layers, although MNF can possibly remove more efficiently the noise from the first components. In particular, ICA provides more contrasted components with less background ghost information from the other paints or the rock wall. This is clearly seen when looking at the two major components (lines 2 and 3 of Fig. 6) which well separate the two main pigments with a smooth background for the ICA while they contain ghost information for PCA and MNF. All the pigment information is also spread over more than 6 components for PCA and MNF while it is concentrated in only 4 or 5 for ICA. This extends to hyperspectral data the higher separation efficiency recently found for ICA compared to PCA on RGB images of rock paintings [69].

Comparison with the DStretch® processing of the exact same area of the context RGB image illustrates the same difficulty in separating paintings and rock: although one component contains only information on rock wall texture and composition (#3, line 4) and contrast is enhanced in the two other components, there is still a strong correlation between them. Hence, there is no effective separation of the pigments, which is mathematically unavoidable in this case due to the limited information contained in the 3 RGB channels. As component #3

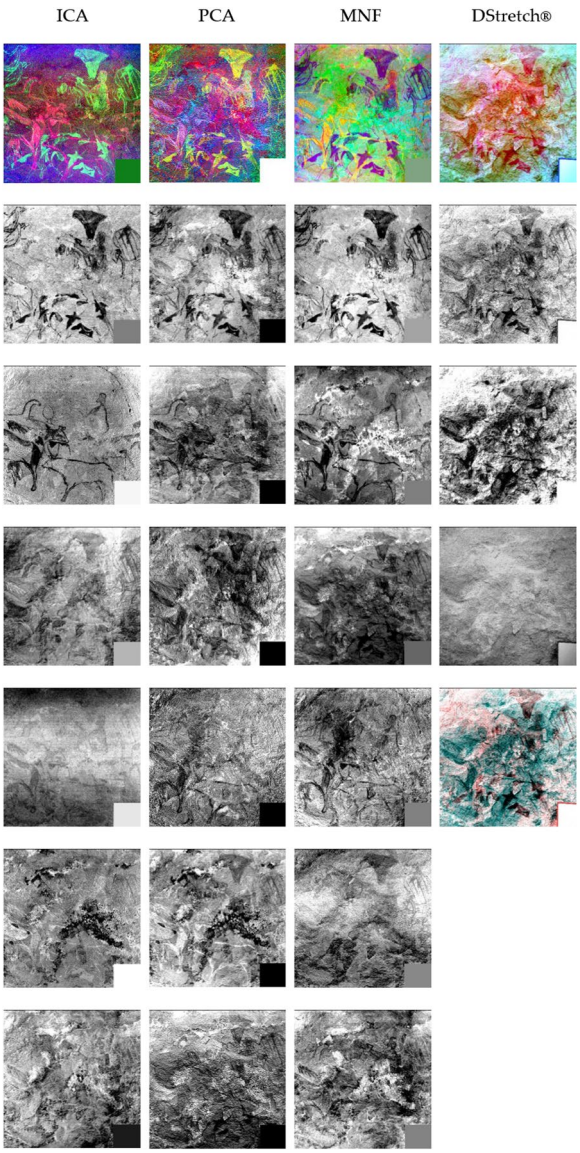

Fig. 6 Comparison between the results of different transformations (ICA, PCA, MNF) performed on one set of hyperspectral data (panel #2, see "Panel #2: Separation between a complex wall and pigments") and with its context RGB image processed with DStretch®. Columns: (1) ICA, (2) PCA, (3) MNF, (4) DStretch®. Line: (1) RGB synthetic image made with the 3 most significant components. Lines (2 to 7) The six most significant components ordered to match as well as possible between the different transformations. For DStretch® there is only 3 components but an improved RGB combination removing the rock wall contribution is given in line 5 (see text). Scale provided by the reference 10 cm square

only contains wall information, a DStretch® RGB image with increased contrast can be obtained by combining only the 2 components containing pigment information, but this did not solve the problem of their separability.

In the following, we mostly used ICA transformation to analyze the hyperspectral data. We first ran a few tests by varying the different free parameters of the iterative ICA transformation which control its convergence (100 iterations with stabilization, contrast function = LogCosh, change threshold = 0.0001) but decided to keep their standard values as they appeared to provide good results with little improvement and much larger calculation times when the convergence constraints are significantly increased. At the end of the calculation, the algorithm orders the ICA components in decreasing order of their spatial coherence (an option in the ENVI algorithm), large scale variations first and purely random noise at the end. This facilitates the separation of those containing useful painting or rock wall information from those mostly or only containing instrument artefact or noise.

From a series of preliminary analyses, all the information that we can identify by visual inspection of the data, as due either to the rock wall or to the paintings, is always contained in the first 10–15 components of the ICA. We thus decided to conservatively run the iterative process of the ICA transformation only on 30 components, in order to reduce the processing time by a factor of 30 (from about 15 to 0.5 min on a powerful 64-bit laptop). The comparison of the results with a full ICA transformation showed no detectable loss of information.

Another tool we will use in this paper is the extraction of end-member spectra characteristic of the purest pixels of each ICA component of interest in order to compare their average spectra and draw conclusions from their differences. They will be selected manually with the help of a thresholding either of the extreme values of each ICA component, and their mean values and statistics will be estimated, or in n-dimension using the 'Pixel Purity Index' (PPI) and n-D visualizer tools. Finally, we will test several spectral classification algorithms, two unsupervised: IsoData and K-means; as well as the supervised Sample Angle Mapper (SAM) algorithm. All these generic tools are available in the ENVI software (and in many others).

Results

Here, we present several results obtained by ICA transformation on a selection of six typical or challenging painted scenes (called "panel" hereafter) of increasing complexity, and compare them with camera images, at both equivalent and very high resolution, processed with DStretch®. These comparisons present different situations for which hyperspectral images bring an improvement compared to RGB images as well as the type of new information which can be extracted.

The first result is that the ICA transformation concentrates most of the useful information contained in the selected 172 spectral channels into only 6 to 12 independent components depending on the complexity of rock wall and diversity of paintings in the image, with the different paintings typically decomposed into 3 to 7 different components mostly depicting the different pigments used. All the remaining components contained different types of noise sometimes with a few ones mixed with faint ghosts of rock wall or painting information already present in the previous components.

Panel #1: simple scene

In Figs. 7 and 8, a typical simple case is presented: a single scene (panel #1) probably painted with a single pigment on a relatively smooth and homogeneous rock wall. Indeed, the ICA transformation of the hyperspectral image concentrates most of the painting information in a single component with only minor local variations depicted in two other components. Those components add little information, just a slightly different hue of pigment in the upper dog, which is confirmed by comparing average spectra of the different figures. When combined in a false color RGB image and compared to the RGB context image processed with DStretch®, it becomes clear that the hyperspectral data allows a better extraction of the spatial distribution of the pigment. Indeed, the main ICA component has a much higher contrast with less background noise than the corresponding component in the DStretched image. This can be highlighted by thresholding and stretching the channel of the DStretched image containing most of the information on the paint, in order to best select the pigment, i.e. removing as much noise as possible without removing pigment information, and comparing it with the same process applied to the main pigment ICA component (#1) (Fig. 7f).

There is a noticeable gain in selectivity with the ICA component as witnessed, for example, by the better definition of the spokes of the wheel of the cart. This allows an easier pigment extraction, using only global image operations, and its superimposition on the original image (or on any other higher resolution RGB image) to restore the painting on the rock wall with a better, and possibly closer to initial contrast (Fig. 8).

A similar quality of pigment extraction can be achieved by using DStretch® and the same type of thresholding and stretching, but on a much higher resolution RGB image, such as the one in Fig. 9, with about 200 times higher resolution (one pixel in the hyperspectral data cube corresponds to about 14 × 14 pixels in this image).

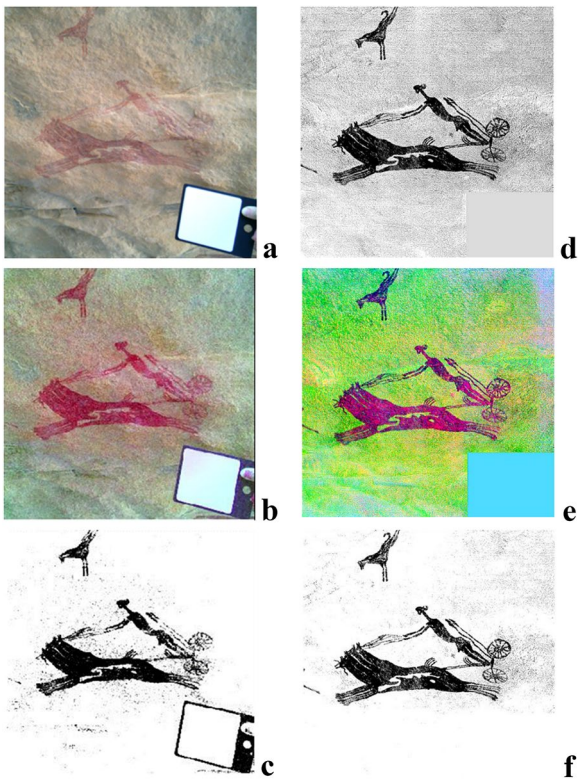

Fig. 7 Comparison of pigment extraction between DStretch® on RGB image (left) and ICA analysis on hyperspectral data (right) on a simple scene (panel #1). **a** Context RGB image. **b** Same image processed with DStretch® (YRD). **d** ICA transformation of the HSI image: the main significant component (#1) containing most of the information on the pigment used in the scene. **e** A false color RGB image using the main ICA component describing the pigment (#1) as well as 2 others recording small local variations (#2 and 6) (R = #6, G = #1, B = #2). **c** the channel containing most of the information on the paint of the above DStretched RGB context image with a threshold and stretch adjusted to select the pigment in the best way, while minimizing the presence of noise. **f** Same but for the main pigment ICA component (#1). Scale provided by the white reference 10 cm square

Panel #2: separation between a complex wall and pigments

Figure 10 provides an example of an effective separation between a complex shelter wall and pigments, as well as discrimination between two overlapping paintings (panel #2). The two main paint components (ICA #1 and 5) are almost completely decorrelated, with only the seated character in the upper right quarter that appears in both components, but as a line drawing in component #5 and as a color filling in component #1. Two other components (#6 and 7) provide additional but more subtle information on the paintings with even fainter and noisier pigment information in component #9. The rock texture is mainly segregated in components #3 and #4. Component #2 is more difficult to interpret given its spatial distribution, but may represent either the remnant of an older painting, or a particular texture of the rock. All other components, #8, #10 and above, are dominated by noise.

Figure 11 displays two end-member spectra of each of the two types of pigments identified, corresponding to ICA component #1 (dark red pigment) and #5 (orange pigment), as well as 2 typical spectra of the rock wall. The spectral differences between them can be recognized, mostly with a stronger absorption below 580 nm and between 750 and 880 nm for pigments, but are relatively subtle especially if one restricts the spectra to the sensitivity range of digital cameras (typically 410–680 nm).

The spectrum of the uncertain ICA component #2 has a less pronounced absorption below 580 nm than the two pigments and most of the rock wall. It mostly occurs where the wall is brighter, but only on part of these brighter area. It may be either an area of 'fresher' less oxidized rock (scraped off?) or covered with a fainter pigment, but apparently covered by the other pigments.

The resulting synthetic 'painting' RGB image using the two main ICA paint components (#1 and #5), together with the secondary component #7, displays different pigments of the paintings much more clearly than the corresponding YWE DStretch® image (Fig. 10).

For this panel, which has at least 2 main pigments with possible local variations, we first tested two unsupervised classification algorithms, IsoData and K-means, but none of them gave satisfactory results on such a complex data set as only the dark red pigment was more or less correctly classified, but not the orange one which is more spectrally similar to the rock wall. We then tested the physically-based spectral classification algorithm Sample Angle Mapper (SAM) on the original spectra of the hyperspectral data cube and on both the MNF or ICA transformations. For the transformations we only used the first significant components (13 for MNF, 8 for ICA) containing information on pigments and rock wall and removed all the noise components. We then used the 'Pixel Purity Index' (PPI) tool in ENVI to find the most spectrally pure (extreme) pixels in the hyperspectral image and the n-D Visualizer to manually select 6 groups of these end-member pixels. The supervised SAM algorithm, using an n-D angle to match pixels to the selected end-member spectra, is then run on the corresponding data and its 'maximum angle threshold' parameter optimized (to 1.0 rad) to classify most of the pixels of the pigments and the rock wall in one of the 6 classes.

The results presented in Fig. 12 show that, as generally stated, the classification of the pigments (3 classes) on the MNF transformation (Fig. 12b) seems more efficient to remove noise than the one run on the ICA (Fig. 12a), but

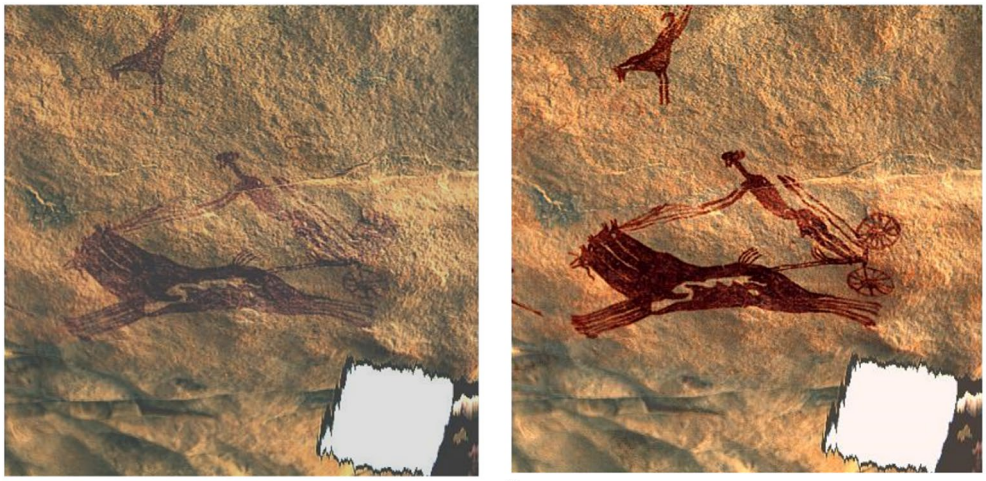

a **b**

Fig. 8 Extraction and restoration of the painted pigments (panel #1): **a** original synthetic RGB image from the hyperspectral data (R = 600, G = 550, B = 450 nm). **b** Same image with the extracted pigment (ICA component #1) superimposed. Scale given in Fig. 7

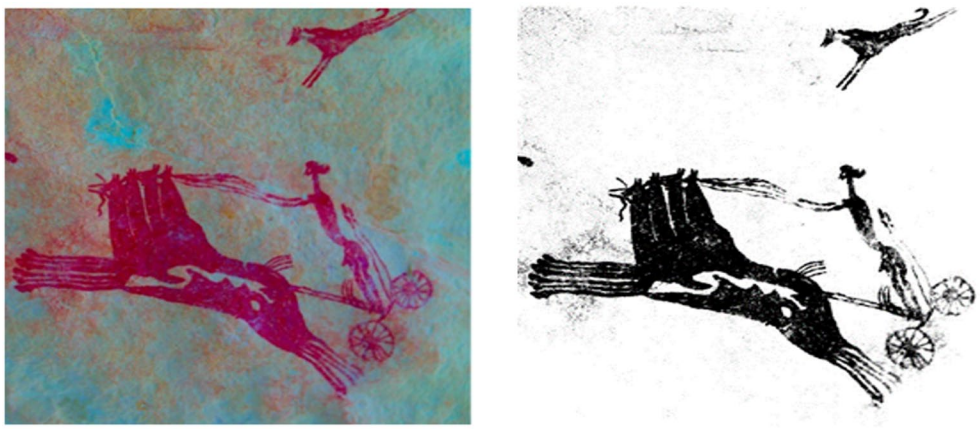

a **b**

Fig. 9 Comparison with a high-resolution image: **a** part of a high resolution RGB image (~ 37 Mpx, ~ 40 µm/px) covering about the same area as Fig. 7 and processed with DStretch® (LRE). The shot angle and point of view of the image were slightly different but illumination was the same as for the HSI image. **b** The green channel of the DStretched image with a threshold and stretch adjusted to best select the pigment. Scale given in Fig. 7

it also misses some faint painting especially in the 'blue' class. Increasing the value of the angle parameter would help include these faint paintings but will also dramatically increase the amount of noise (from wall) in the pigment classes. We should also note that the classification directly performed on the hyperspectral data cube (not shown) is not able to correctly extract most of the pigments for this scene painted on a complex wall. A transformation to concentrate the information and segregate most of the noise is thus really necessary before any classification.

However, we found that an alternative and more efficient way to classify the pigments is to capitalize on the high separation power of ICA by simply thresholding its main components depicting the pigments (Fig. 12c), the corresponding end-members being the most extreme pixels of each ICA component. The results show that this method provides a slightly better recovery of the pigment distribution obtained by SAM classification of ICA (Fig. 12a) and much better than the classification performed on the MNF, but with a noise level as low as that of MNF (Fig. 12b).

The first advantage of this method is that it is easier (interactive on most software), faster and more objective, to determine the parameter value that is the best compromise between pigment separation and noise

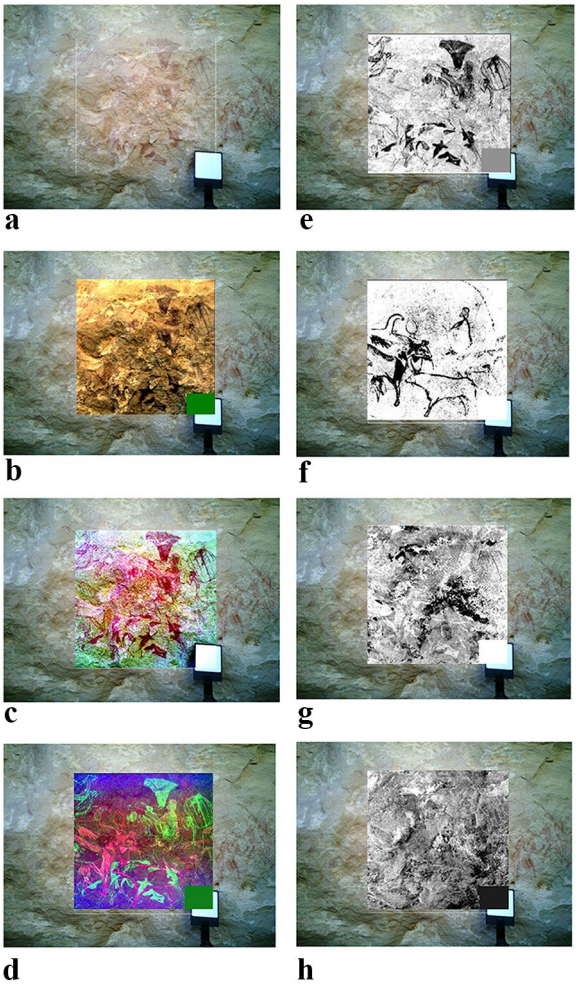

Fig. 10 Separation between a complex shelter wall and pigments, and discrimination between two overlapping paintings (panel #2). **a** Context RGB image. **b** Synthetic RGB image of the HSI data (R = 600, G = 550, B = 450 nm). Right: ICA transformation of the HSI image: the 4 most significant of the 8 components containing information, the top two (**e**, **f**: ICA components #1 and 5) separates two different pigments. **g** Depicts an unidentified component (#2): paint or wall? **h** ICA component (#4) that extracts part of the complex texture of the underlying rock wall. **d** Synthetic RGB image using 3 ICA components (R = #5, G = #1, B = #7) displaying the different pigments (in red and green) much more clearly than the corresponding DStretch® (YWE) image (**c**). Scale provided by the white reference 10 cm square

contamination. Another advantage is that it has not the restriction of the 'exclusion principle' of all classification tools (one pixel can belong only to one class) and thus it allows to have pixels in two or more classes where two pigments are mixed or superimposed, an important information that should not be discarded. In Fig. 12c it is particularly the case of the human figure in the top right part of the scene where a drawing with the orange pigment (ICA #5, blue class) is superimposed with solid dark red pigment (ICA #1, red class), unlike almost everything else on the scene (see also Fig. 10e, f). And finally, the extraction of each pigment can be optimized by its own threshold value of the ICA component, contrary to SAM classification (and many others) where a unique and common value applies for all classes.

Panel #3: highlighting invisible/barely-visible figures on complex rock wall

Another interesting example is a strongly oxidized brown–red wall with barely visible traces of red pigment on top of the image (panel #3, Fig. 13). The DStretch® (YUV) processing of the context RGB image allowed us to confirm the presence of several figures at the top of the image and possibly a bovine in the middle-left. The ICA analysis of the HSI image clearly displays these figures in components #2 and #7, but components #5 and #4 uncovered in a very clear way a few large anthropomorphic figures belonging to another layer of painting that is unobserved by eye. These figures remained undetected on the context RGB image despite a whole set of analysis attempts using various options of DStretch®, as well as different types of stretching algorithms (Photographic stretch, Saturation stretch, Decorrelation Stretch), transformation algorithms (PCA, ICA, MNF) and anomaly detection algorithms (RXD, UTD, RXD-UTD) available in ENVI software. Only the 'elongated head' of the main anthropomorph can be barely recognized a posteriori in some of these transformations. With the ICA of the HSI data the different types of rock texture and composition are also well separated in components #1, #3 and #6.

Even with a high-resolution camera image (60 Megapixels) covering part of the hyperspectral dataset and processed with DStretch® (IDS) or the other algorithms we can hardly recognize some of the 'anthropomorphs' elements, even knowing where they should be located in this stretched image (Fig. 14). They only have a very slightly different orange hue in this stretched image compared to the surrounding oxidized rock with strongly variable hues.

A comparison of end-member spectra of the three main ICA components of panel #3 and of the rock wall (Fig. 15) shows only little variability between the pigments and the oxidized rock wall, in particular in the 400–600 nm range where the oxide absorptions are very similar among the spectra. The spectral features that should mainly contribute to the detection of the painting of the large anthropomorphs are most probably the slightly more marked shoulder around 590 nm and the flat part of their spectra between 770 and 850 nm which strongly contrasts with the steady spectral slope of the rock wall. Moreover, its separation from the other pigments occurs in the visible range (stronger slope and curvature between about 500

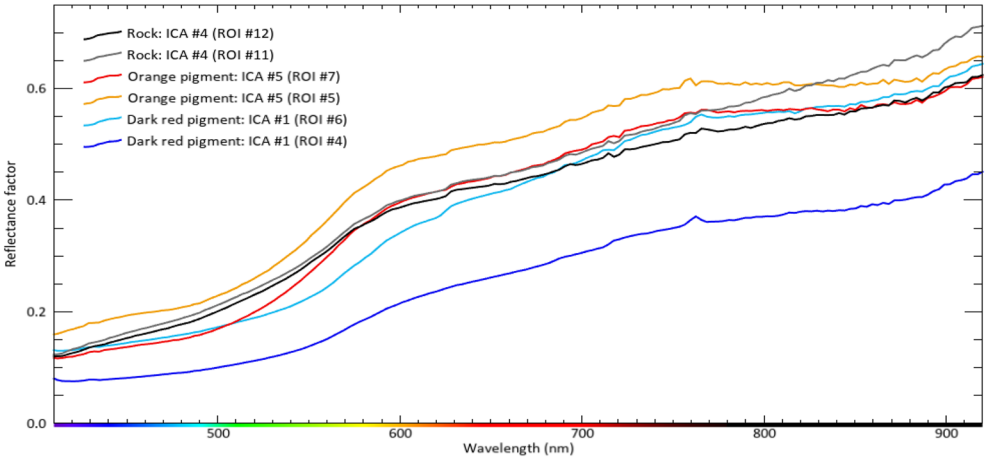

Fig. 11 End-member spectra (average of 30 to 100 pixels) of the orange pigment (red, orange) and dark red pigment (dark and light blue) and typical spectra of the rock wall (black and grey) taken from the hyperspectral image of panel #2 presented in Fig. 10

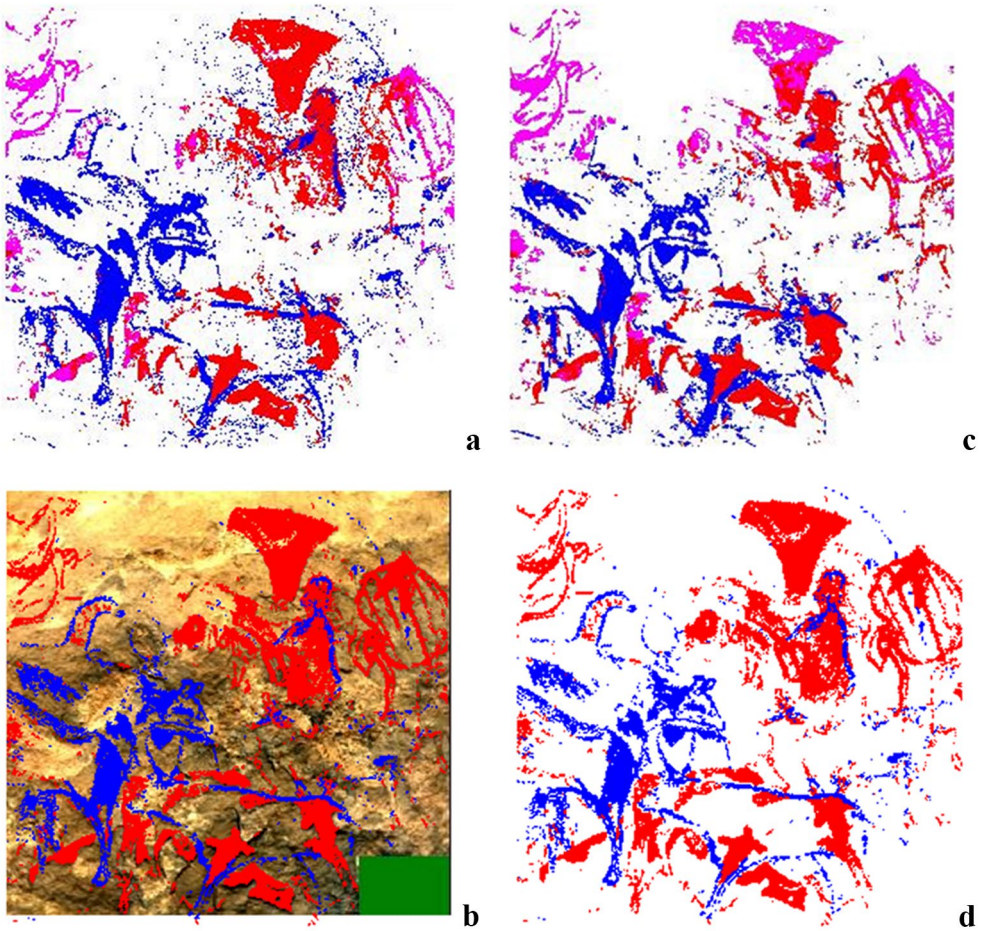

Fig. 12 Classifications of the pigments from the hyperspectral image of panel #2. **a** Run on the 8 first components of the ICA transformation. **b** Run on the 13 first components of the MNF transformation. In both cases 6 groups of end-members pixels were selected with the 'Pixel Purity Index' (PPI) and n-D visualizer tools in ENVI before Sample Angle Mapper (SAM) classification. Only the 3 classes depicting pigments are shown here. **c** Classification obtained by thresholding the 2 main ICA components (#1 and 5) of the painting. The blue class (orange pigment) is plotted over the red (dark red pigment). **d** Same superimposed on the context image. All 3 classification were post-processed with a slight 'sieving' algorithm (with a pixel connectivity of 8 and a minimum size of 4) to clean part of the random noise disconnected from the painting

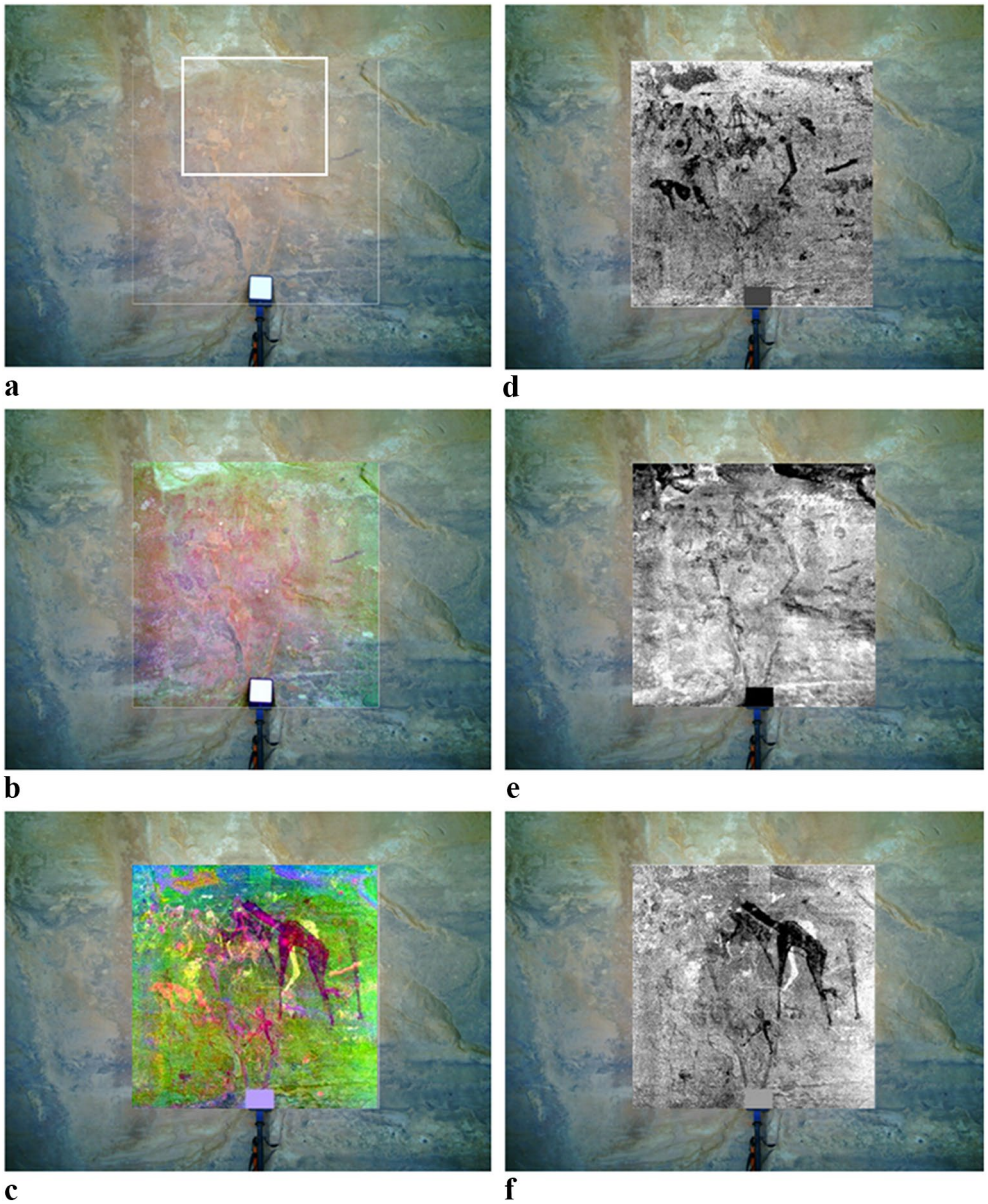

Fig. 13 Highlighting invisible figures on complex rock wall (panel #3). **a** Original context RGB image. Right **d**, **e**, **f**: ICA transformation of the HSI image: the 3 most significant of the 7 components with information (ICA components #7, 2 and 5) clearly separating three different pigments. **c** Synthetic RGB image of the HSI data using the 3 ICA components (R = #7, G = #5, B = #2) displaying the different pigments. The large anthropomorphs are mostly invisible in the corresponding DStretch® (YUV) image (**b**), only the 'elongated head' of the main anthropomorph can be barely recognized a posteriori. Scale provided by the white reference 10 cm square. The rectangle in the image b locates the high-resolution image of Fig. 14

and 580 nm) where the anthropomorph's pigment has a color and a spectrum very similar to the rock wall. This explains why an RGB camera cannot distinguish these figures from the oxidized background wall.

For a better assessment of the relative contributions of the visible and near-infrared regarding the figures versus the rock wall respectively, we performed ICA transformations on different spectral subsets of the HSI data, i.e. the visible spectrum only and the near-infrared spectrum only.

The transformation over the visible spectrum was limited to the 93 spectral channels contained in the photopic sensitivity range of the human eye (420–675 nm, i.e. for sensitivity > 2% of its maximum [32]). While still clearly identifying the anthropomorph figures, their contrast with the surrounding is partly

Fig. 14 High resolution camera image (60 Mpx, ~ 65 µm/px) processed with DStretch® (IDS) and covering part of the hyperspectral dataset (panel #3) presented in Fig. 13. The point of view is slightly different than for the HSI image. Even knowing where the 'anthropomorphs' painting occurs in this stretched image we can hardly recognize some of its elements from the very slightly different orange color compared to the surrounding oxidized rock. Scale and location given in Fig. 13

reduced and some small parts are missing (Fig. 16b). Other figures, such as the bovine in the middle left of the image and the series of characters above, are much less clearly detected using only the visible range (Fig. 16c, d).

The ICA transformation restricted to the near-infrared, performed over the 73 spectral channels of the 700–920 nm range, displays all painted figures in a single component with the anthropomorphs less sharply defined but containing the missing parts in the visible range, and with all the other painted figures with high contrast relative to the rock wall (Fig. 16e).

These tests show that the visible and near-infrared ranges contribute in different but complementary ways to enhancing the contrast and separation of the figures in the full spectrum result. The visible range appears to play a major role in the separation between different painted figures while the infrared range mostly boosts the contrast between the figures and the rock wall.

A final test, aimed at better understanding the limitation of RGB images in detecting very faint figures, was performed using only the three spectral channels corresponding to the RGB peak sensitivity wavelengths of either the eye (~ 421, 530, 558 nm) or the camera (~ 470, 530, 600 nm). In the case of the eye peak wavelengths the ICA transformation slightly highlights the anthropomorph figures (Fig. 16f), while in the case of the camera, only the series of characters on top left of the image is highlighted. The large width (60–100 nm) and strong overlap of the RGB sensitivity curves of the eye and of standard cameras with respect to the narrow spectral bands (7 nm wide) used here are most likely the main factors that prevent them from distinguishing pigments that have both close color and very low contrast.

Panel #4: discovery of indistinguishable painting and separation of paint layers

An even more complex situation is represented by the hyperspectral image of panel #4, where a Barbary sheep is easily seen with naked eyes, as well as two greenish lines on the top left quarter of the image (Fig. 17a).

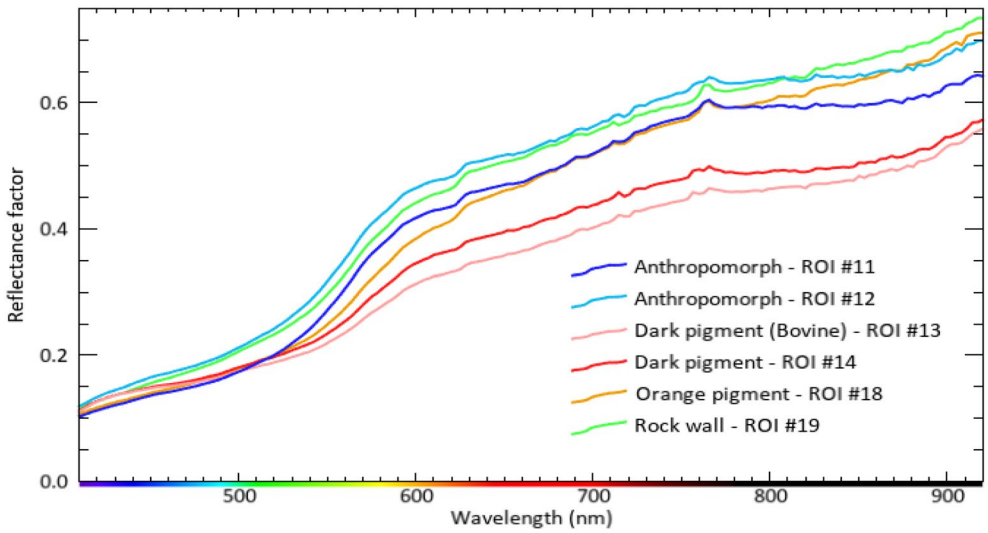

Fig. 15 End-member spectra (average of 40 to 110 contiguous pixels) of the orange pigment (orange), the dark red pigment (light and dark red) and the anthropomorph pigment (dark and light blue) and typical spectrum of the rock wall (green) selected in the hyperspectral image of panel #3 presented in Fig. 13

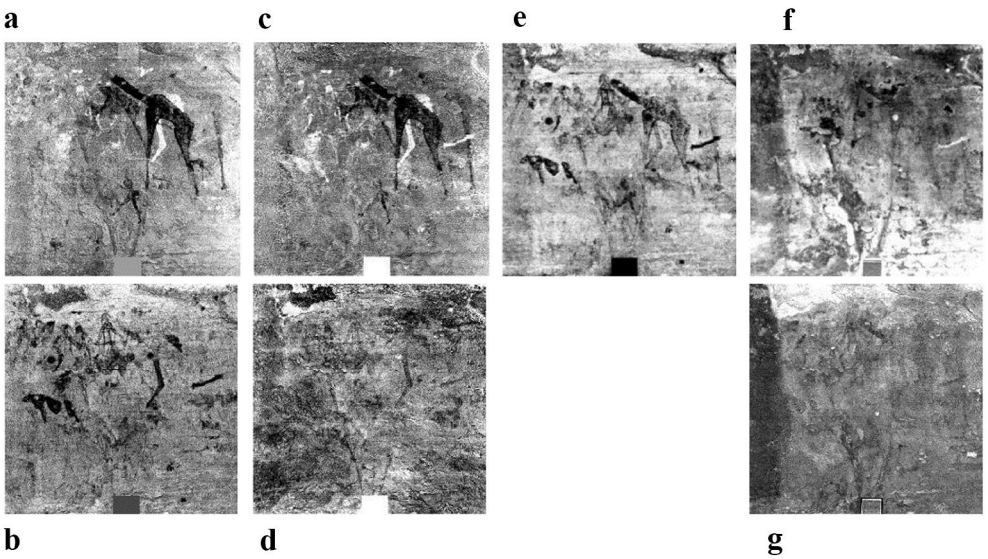

Fig. 16 The main components of ICA transformations of the hyperspectral image of panel #3 performed on **a**, **b** the whole spectrum (410–920 nm, from Fig. 13), and on different subsets of the spectrum: **c**, **d** the visible spectrum only (420–675 nm), **e** the near-infrared spectrum only (700–920 nm), and **f**, **g** the three RGB peak sensitivity wavelengths of the eye (~421, 530, 558 nm)

Processing the RGB context image with DStretch® confirmed these observations but did not reveal more figures. The ICA analysis of the corresponding hyperspectral image (Fig. 17) reveals 3 superimposed paintings or drawings separated in 7 information components (#1 to #3, #5 to #7 and #9). In addition to a part of a second Barbary sheep on the right side of the image, the outline of a large anthropomorph, of which only the tail and part of the back are visible in the camera and DStretched images, now more fully appears all around the first Barbary sheep. However, some parts of the contour lines of the anthropomorph are still hidden below the two Barbary sheeps making this outline very spotty at some places and surrounded by a variety of rock colors and more recent paintings. DStretch® cannot highlight it as its statistics for stretching focuses on the dominant colors of the image in terms of covered surface, i.e. the Barbary sheep painting and the highly variable rock wall colors.

The outline of the Barbary sheep is also well separated in the ICA components from its filling, probably drawn with another pigment or technique. All these paintings can be represented in a false color image by combining 3 of the ICA components (R = #3, G = #6, B = #9) (Fig. 17d). It shows that in addition to these main figures a few other painting, or part of paintings, are also present, such as a third horned 'ghost' left of the head of the first Barbary sheep (in green in Fig. 17d), or additional lines above the back and below the right hand of the 'siemen' anthropomorph (in faint pink in Fig. 17d).

There is also a 'goat' with thin horns and legs that looks like it is scraped on the rock (bright lines), partly over the Barbary sheep. It can be already guessed in the original context RGB image from some lines and area whiter than the rock and locally removing the pigments of the Barbary sheep (Fig. 17a). However, the ICA transformation extracts its component with little contrast relative to the background. An MNF calculation was also run on this image, which provided a component with a better contrast and signal to noise ratio allowing us to better determine the outline of the 'goat'. A false color RGB image of the 3 main MNF components (Fig. 17h) clearly shows the superimposition of the three paintings or drawings.

In the case of this panel the MNF transformation, although not efficiently separating the different pigments, provides interesting complementary results. In particular some of its components clearly display two or three of the superimposed paintings, more efficiently cleaned from the complex rock texture (Fig. 18).

The MNF components can be an additional help to understand the paintings organization and sequence, e.g. we can now spot a small figure behind the first Barbary sheep, inside the thigh of the anthropomorph, which is seen only in secondary painting components of the ICA (with fainter and noisier information) and thus not visible in the synthetic RGB images of the main painting, such as the two images of Fig. 17d, h. A specific analysis of these secondary component is necessary to highlight this figure (Fig. 19) and the MNF component provides a slightly sharper view.

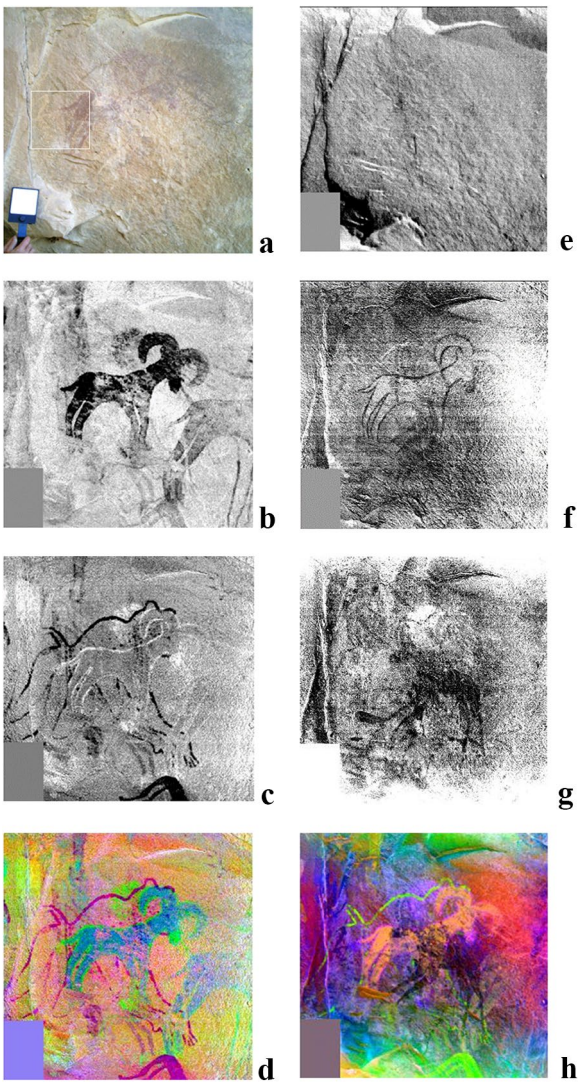

Fig. 17 Discovery of an indistinguishable painting and separation of three layers of paints (panel #4): **a** original context image. Middle rows: ICA transformation of the HSI image: the 4 most significant components (**b** #3, **c** #9, **f** #6, **g** #1) of the 7 components that separate at least four different pigments. **e** ICA component (#4) of the 'cleaned' rock wall. **d** False color RGB image using 3 of the pigment ICA components (R = #3, G = #6, B = #9) displaying two of the 3 superimposed drawings (in red and blue-green). **h** False color RGB image using 3 components of a MNF transformation (R = #2, G = #3, B = #6) highlighting the superimposition of the 3 paintings. Scale provided by the white reference 10 cm square. The rectangle in the context image locates the zoom presented in Fig. 1

The shape of the end-member spectra collected for the main four pigments provides an overview on how they can be differentiated (Fig. 20). Again, the main spectral features that should allow to separate between these pigments are located in the 500–650 and 750–900 nm ranges. In particular, the shoulder around 580 nm for the anthropomorph is shifted up by about 20 nm for the Barbary sheep pigment, and in addition, it has a lower slope than typical surrounding rock below 500 nm and above 590 nm. So, contrary to the anthropomorph of panel #3, its pigment can be clearly differentiated from the others and from the surrounding rock by its color. It is indeed the superposition of the other two drawings and the overall complexity of this panel that makes the outline of the anthropomorph of panel #4 very difficult to perceive. The difficulty is here more a question of detectability of the discontinuous silhouette of the anthropomorph than of visibility of its pigments.

As for panel #3, we also tested the relative contributions of the visible and near-infrared ranges by performing ICA restricted on these two ranges (not displayed). In the case of panel #4 the different figures are readily separated using only the visible range, but the near-infrared seems to contribute better to recover the faintest paints with a more efficient separation from the rock wall.

The hyperspectral image presented above (Figs. 17, 18) is part of a series of three images which cover a larger part of panel #4 and depicts several superimposed scenes painted with different styles when analyzed with ICA and subsequently projected (with 2D-spline adjustment on a large number, ~ 40, of common anchor points) and merged on a high-resolution image of the same rock wall (Fig. 21). As a first approach the ICA transformations were performed independently on the three hyperspectral images (with their own statistics) but they provided quite consistent components that can be easily matched.

The overall organization of this panel is very complex with numerous overlapping figures that probably belong to more than 3 layers. A complete analysis would need to also study in detail the other 5 components containing pigment information and displaying other fainter figures, but this is out of the scope of this paper. We can nevertheless point a few additional interesting results. In particular two other types of anthropomorphs, which can already be seen in the other parts of panel #4 in the DStretch® image (the Fig. 21c) are also well extracted and appear to be painted with a similar pigment as the first one. The 'simen' anthropomorph style, at the bottom part of the panel, is however only partly seen in the DStretched image, its head and back being hidden by a large rock scarp clearly visible in the bottom quarter of the RGB image (Fig. 21a). In contrast, the whole figure is well seen in the ICA component despite the interference of this large rock default.

Panel #5: the case of white painting

A known difficult case where DStretch® struggles to improve contrast is the presence of faint white paints, due to a lack of tint. We tested the detection and

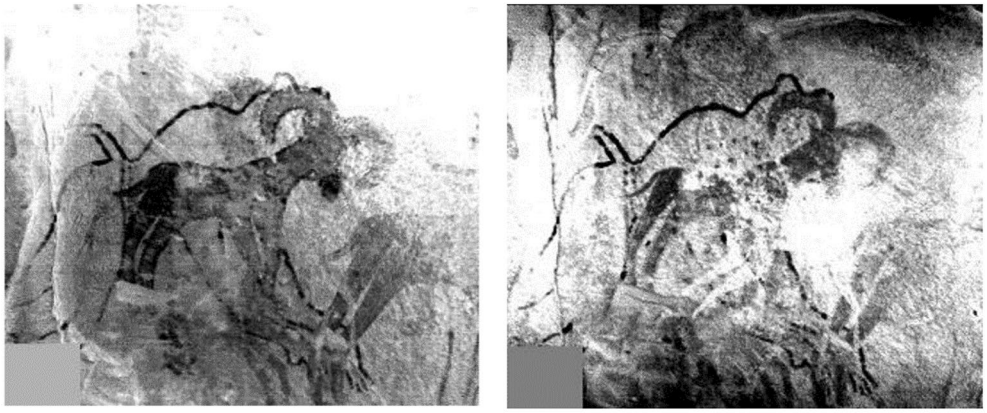

a **b**

Fig. 18 Two components of the MNF transformation (panel #4) displaying the superimposition of several painting layers, with smoothed rock wall texture. **a** The anthropomorph (first layer) and the Barbary sheeps with their outline (second layer). **b** Same (but without the Barbary sheep outline) with the addition of the goat as the third 'layer'

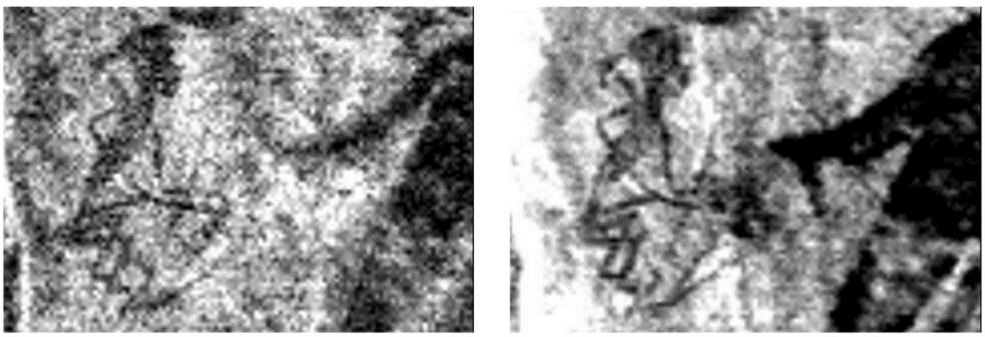

a **b**

Fig. 19 Zoom of a small part of panel #4, highlighting a small figure only seen in the ICA components containing secondary information (#2, #5, #7, #8). **a** ICA 'secondary' component #2. **b** MNF component #4 displaying a slightly better signal-to-noise ratio and thus a better figure definition. Scale and location given in Fig. 17

separation of faint white painting to assess if a VNIR HSI instrument can better extract such colorless pigment from the others and from the rock wall. Figure 22 shows a faded-out scene comprising a complex mixture of various pigment colors, including whitish (panel #5). The scene is decomposed in 4 main ICA components (#1, 3, 4, 6) for the pigments, the first one representing the whitish paint (Fig. 22d**),** the second the upper left bovine and the two last ones the three other bovines. However, although component #1 clearly improves the visibility of the faintest white figures (see in particular the barely visible thin human figure close to the right edge, above a bovine), the contrast with the surrounding wall and the other paintings is not as sharp as that obtained in the previous panels for orange or red pigments. Also it does not significantly improve the visibility of the whitish figures already visible with naked eyes (see e.g. the second human figure from the right edge).

Comparison of the synthetic RGB image build using the 3 first painting ICA components (#1, #3, #4—Fig. 22d–f**)** against the context image processed with DStretch® LAB (Fig. 22c) shows that the ICA decomposition provides a significant contrast improvement of the faintest whitish pigments. We should note here that the specifically designed 'white' YWE and LWE DStretch® enhancements were not well working with this scene.

We then compared the spectra of the whitish human figures with the surrounding wall and the two types of bovine seen in the ICA components #3 and 4 (Fig. 23). We can see only little difference in spectrum shape of the two

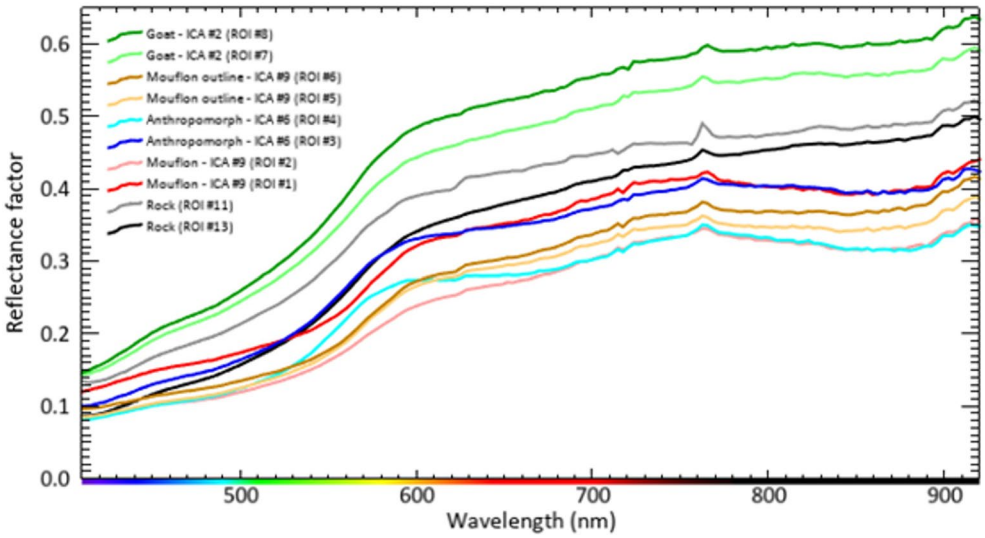

Fig. 20 End-member spectra (average of 35 to 75 pixels for pigments, > 300 for rock) of the Barbary sheep pigment (light and dark red) and its outline (orange and brown), the anthropomorph pigment (dark and light blue), the goat (light and dark green) and typical rock wall area (grey and black) selected in the hyperspectral image of panel #4 presented in Fig. 17

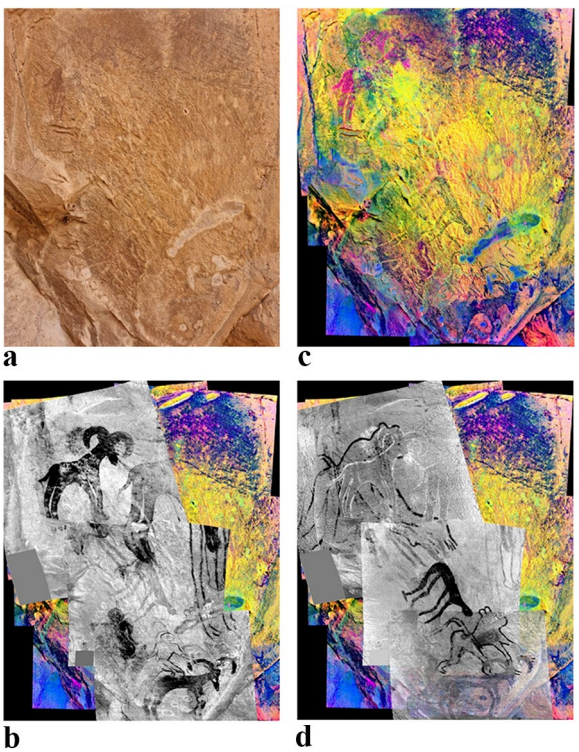

Fig. 21 The two main scenes of a larger part of panel #4, separated using the ICA transformation and projected on a high-resolution image of the whole panel (Samsung galaxy S21, 64 Mpx). **a** RGB high-resolution camera photo (slightly different shot angle but same illumination as for the HSI image). **c** YBK DStretch® processing of a stitching of several high-resolution photos. **b** The 'Barbary sheep scene' build with 3 hyperspectral images analyzed with ICA transformation (component #3). **d** the 'anthropomorph scene', same but using ICA component #6

whitish human figures with the nearby rock wall, especially for the faintest one which has its spectrum exactly overlapping that of one of the rock (grey spectrum) up to 560 nm and little departure (< 0.02 in reflectance) in the remaining visible range. The main difference with the underlying wall is a more pronounced shoulder around 580 nm leading to about 15–20% brighter reflectance in the very near infrared. These whitish human figures are in fact not so white, but rather reddish according to their spectra, but they look whitish only by contrast because they are slightly brighter than the wall, especially figure #2, contrary to most red paints that are darker, as it is the case for the bovines. Part of the human figure #1 has color and visible brightness so close to the surrounding wall that only small dotted parts are visible by contrast to the eye. It has also a more reddish color than figure #2 (slightly stronger spectral slope below 450 nm) as it also appears in the ICA component #4 which mostly depicts the light brown part of the bovine below (Fig. 22f). Some of the bovines are also difficult to discern with naked eyes due to very similar visible spectra of the surrounding wall (in particular, the one in the upper left quarter of the image), but they have clearly different spectral shapes outside the eye sensitive range, in particular between 680 and 900 nm, which allow the ICA to extract them with a much sharper contrast with the rock (Fig. 22e, f).

Panel #6: separation of graffiti superimposed on paintings

A final example of the ability of VNIR hyperspectral imagery coupled with ICA transformation to separate different information mixed together on the rock is the

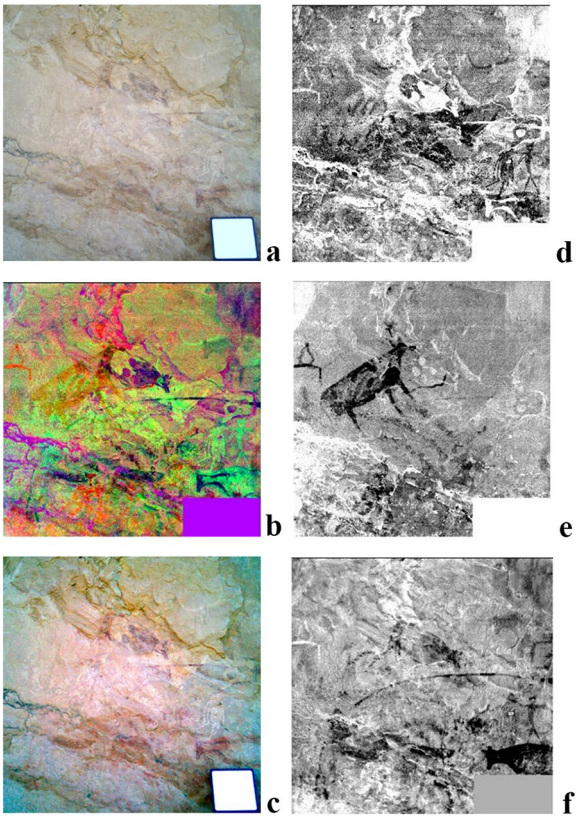

Fig. 22 Detection and contrast improvement of faint white painting (panel #5). **a** Original RGB context image. Right: ICA transformation of the HSI image: the 3 most significant ICA components (**d** #1, **e** #3, **f** #4) describing the painting. **b** a synthetic RGB image using these 3 painting ICA components (R = #4, G = #1, B = #3). **c** DStretch® (LAB) image for comparison. Scale provided by the white reference 10 cm square

case of 'modern art and poetry' superimposed on Neolithic painting.

Figure 24 shows a painting 'contaminated' with several graffiti drawn with different materials and colors (panel #6). The ICA transformation of the hyperspectral image produces 12 significant components with information on the relatively complex painting (5 components: #5 to #9), the rock wall (3 components #3, #4, #10) and the graffiti (2 components #1, #11) as well as 2 components with mixed information (#2, #12).

When simulating a false color RGB image of the painting using three of the five components with relevant information, the graffiti can only be barely seen in the image (Fig. 24b) most of its information being concentrated in ICA component #1. The PCA transformation is found to be slightly less efficient to segregate the graffiti information in this hyperspectral dataset (Fig. 24f), and a MNF transformation did not separate efficiently enough painting, rock and graffiti to be useful in that case. DStretch® applied on the RGB context image is also completely unable to remove the Graffiti (Fig. 24c). At the opposite it has the tendency to highlight them to the detriment of the other colors.

Discussion

Even with a spectral range limited to 410–920 nm, mainly due to measurements of shaded walls indirectly illuminated by sunlight scattered from the sky and reflected by the surrounding landscape, the analysis of the hyperspectral data cubes provided many improvements over DStretched RGB camera images. The main advantages of hyperspectral imagery for the study of Neolithic paintings can be listed as follow.

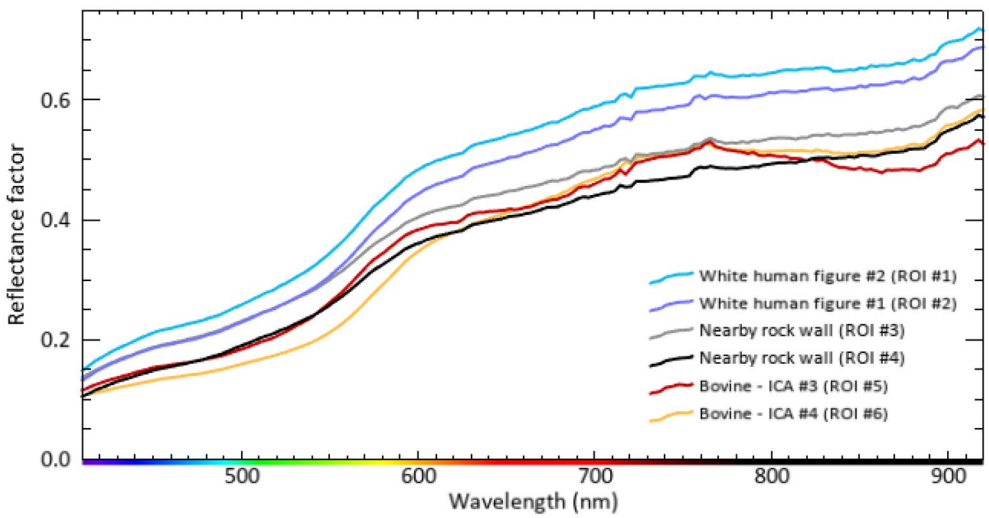

Fig. 23 End-member spectra (average of 35 to 75 pixels for pigments, > 300 for rock) of the whitish human figures (dark blue: #1, light blue: #2) with the surrounding wall (grey and black) and the two types of bovine seen in ICA component #3 and 4 (orange and red) of panel #5

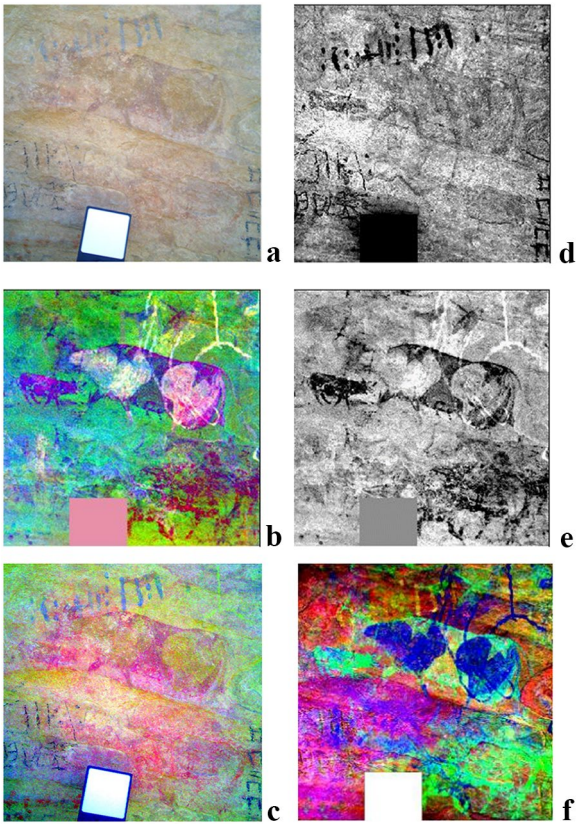

Fig. 24 Separation of *'modern art and poetry'* superimposed on Neolithic paintings (panel #6). **a** Original RGB context image. **d**–**e** ICA transformation of the HSI image: 2 of the 12 significant ICA components, d) component #1, clearly separating the graffiti. **e** One (#6) of the five components describing the painting of this relatively complex panel. **b** A synthetic RGB image using 3 of these 5 'painting' ICA components (R = #8, G = #6, B = #7). The graffiti can only be barely seen in this image, most of its information being concentrated in ICA component #1. **c** DStretch® (YDS) image for comparison. **f** The best synthetic RGB image of PCA components still displaying some ghosts of the graffiti. Scale provided by the white reference 10 cm square

First, based on ICA analysis which concentrates the useful information in 8 to 12 components, with 3 to 7 concerning pigments, we could better separate different physical contributions to the image which are generally mixed in the three channels of a standard camera, including:

- The pigments and the underlying rock.
- The composition (mostly Fe-bearing minerals) and the color of the pigments.
- The different paint layers and their juxtaposition.

While ICA is relatively efficient in separating different types of pigments used (independent components), it did not provide by itself composition information. This can be obtained from the end-member spectra of the components by comparing them with laboratory spectra of well characterized pigments or minerals [50]. However, with the VNIR range we can only provide information on the Fe-bearing minerals. SWIR would be necessary to get info on some of the other minerals, such as kaolinite, carbonate and sulphates, constituting the paintings.

We could detect faint paintings, which were undetected by the naked eye and even with high resolution camera images post-processed with DStretch®. In the various cases studied we found different reasons that led the ICA analysis of hyperspectral data to highlight new figures. In one case (panel #3) the pigment of the figure, an anthropomorph, has a color too similar to the complex surrounding rock to be separated by eye or by a DStretch processed RGB image, but it can be easily differentiated in the very-near infrared thanks to different spectral behaviors. The situation is similar for panel #5 (a whitish human figure) but occurs even in the presence of a fairly homogeneous wall color. In both cases the 'near-infrared vision' provided by the HSI instrument is key to detect these invisible figures. In another case (panel #4) the paint was faint but sufficiently contrasted in the visible range relative to rock. However, the superimposition of at least two other paintings crossing the first one in many places led to very discontinuous and faint remains that the eye was unable to recognized as a painted figure in the middle of a complex mix of other figures. The ICA extraction of this paint layer from the other layers and from the rock texture allowed us to obtain a clean image of the visible remains of its paint, completed by additional missing pieces located under other thin paint layers.

Thus, specific spectral ranges contribute the most to differentiate the pigments from the rock wall (e.g. panel #2, Fig. 13), or between 2 pigments. However, in some cases only very subtle spectral differences are noticeable (e.g. panel #3, Fig. 15 and panel #5, Fig. 23). These sensitive ranges are not always the same and depends on the painting, its alteration as well as the weathering of the rock wall. In our cases the two most sensitive ranges are both in the visible, around 580 nm, and in the near-infrared, above about 750 nm. It is why not only the whole wavelength range needs to be used, but also the analysis of various cases with no preconceptions on which type of spectral difference exists between pigments and rock wall textures.

While both ranges contribute to enhance the invisible or very faint figures, we found that the visible range plays a major role in the separation between different painted figures while the infrared mostly improve the contrast between the figures and the rock wall.

The extraction and efficient separation of the different painting layers is the second major advantage of hyperspectral data, as soon they have some spectral differences in the VNIR spectral range, either due to differences in e.g. color, composition, texture, thickness or alteration.

Due to the numerous spectral channels and the wider spectral range, the ICA transformation allows us to suppress or reduce the effects of the rock wall structure and of the inhomogeneous lighting. It can also remove a large part of the noise in the image and thus increases strongly the contrast between the paint itself and its surrounding environment. The example of panel #1 shows that even a small HSI instrument with just 0.25Mpx can compete with large cameras with several dozen Megapixels in terms of pigment extraction thanks to the efficient segregation of instrumental (from the HSI camera) and natural noises. This later 'noise' is in fact produced by high frequency spatial variations of reflected light induced by the rock and paint textures at microscopic/millimetric scales and some larger scale lighting variations, both factors that cannot be suppressed even with very high-quality cameras. Indeed, the pixel size of this HSI instrument (about 1–2 mm depending on camera-wall distance) is still slightly larger than the sub-mm size of the textural unit (grain facet) of sandstone rock, but the pixel size of high-resolution cameras (10–100 µm) may be smaller than crystal facets. So 'single grain BRDF' (and probably mostly its specular component) begins to be a major factor of pixel-to-pixel variability in high resolution images. It should be noted that the intensity of these fluctuations is greatly reduced in diffuse light (such as in shaded area) compared to direct sunlight (or artificial light) because of the angular spreading of the microscopic specular reflections (first external reflection at rock crystal face scale) and the attenuation of shadows at all scales. So, the reduced amount of light and the slightly limited spectral range in the shadowed area may be partly compensated by the diffuse lighting leading to the removal of a large part of natural 'textural' noise. The advantages of VNIR HSI acquisition in full sunlight is mostly the acquisition time which may be reduced to less than 1 min (instead of 3–10 min in shadowed area), and the extended spectral range up to 1000 nm which may probe additional differences between near-infrared spectra. But the stability of the measurement, in terms of absolute intensity and, more critically, color (white clouds versus blue sky) is then highly sensitive to any cloud moving in the vicinity of the sun direction. The respective advantage of the two situations in terms of pigment detection and extraction performance has yet to be assessed in a range of relevant situations.

The ICA decomposition on VNIR HSI data may also detect pigments under another paint layer where this layer is thin enough to be translucent in the very near infrared (>700 nm), where most chromophore mineral pigments are less absorbing (see e.g. [50]). In addition to uncovering parts of an underlayer figure, this ability of HSI may also be to 'clean' graffiti drawn over Neolithic painting, such as in the example of panel #6.

Pigment classification is a further step in the analysis of a painted prehistoric scene. Our first tests with the simplest algorithms (IsoData, K-means, SAM on MNF and ICA transformations) show that the most satisfactory is SAM on MNF but our simpler classification technique of thresholding ICA components proved to be more efficient in classifying the two main pigments while further limiting the interference of background noise. This method also has the advantage of allowing quick and easy adjustment of a single, independent parameter for each component to obtain the best compromise between pigment separation and noise elimination. It also frees itself from the 'exclusion principle' of all classification tools and thus keep the very important information of the location of mixed or superimposed pigments.

More sophisticated classification algorithms may possibly get slightly better results, and should be tested in the future. However, they are generally more complex and time consuming, with pre-processing steps (extraction of end-members…), and parameters, sometimes purely mathematical, to tune to each case by trial and error. And in most cases the classes are constrained by the 'exclusion principle'.

We also note some limitations in the measurement presented here, such as the format and spatial resolution of the HSI images. Although such lightweight and stand-alone VNIR HSI camera is ideal for exploratory campaigns, a larger hyperspectral image format is necessary to make comprehensive surveys at higher spatial resolution of extended Neolithic or Paleolithic sites. Such instruments have been around for more than a decade and have recently been extended to a 3000-pixel swath leading to hyperspectral images of more than 15 megapixels. However, they require heavier logistics in terms of scanning system, set of front optics, computer and power supply.

Extending to the near infrared (SWIR: Short-Wave InfraRed, 1000–2500 nm) might also improve the separation between paints and rock and should also provide additional information especially on the composition of pigments and on the taphonomy of the rock wall (see e.g. [50, 70], but the logistic (and cost) of SWIR HSI instruments is even heavier, in particular in weight and energy consumption, which should be considered for remote field operations.

Alternative solutions to VNIR HSI may be multispectral VNIR cameras with 8 to 20 spectral bands

and larger image format if they cover a wide enough spectral range (at least 400–900 nm) in order to be sensitive to some very near infrared spectral differences between pigments and/or rocks of same apparent color (see e.g. panels #3 and #5). The simplest ones with only 8 spectral channels (using a 3 × 3 Bayer filter mosaic) may already provide useful additional information, but as they still strongly under-sample the whole spectral information, the separation between pigments, rock and noise will not be optimal in the case of complex paintings and /or rocks. Although we have not fully investigated the effects of number, position and width of spectral channels, our guess, given the number of useful information channels, is that instrument noise and natural high spatial frequency fluctuations will not be well segregated by the ICA transformation until a large number of spectral channels (> 20) is used. Indeed, in our study up to 12 components contained useful information and the noise was concentrated in the other ones.

Another aspect to be considered is the processing of the hyperspectral data, which is more complex and computer and manpower time consuming as it involves copy of the data set to a computer, preliminary inspection of the data to optimize the process, a series of high-level mathematical operations on the data cubes to get the results, followed by visual inspection of each of the 12–15 first ICA components to determine which type of information they contain (painting, rock, illumination field, noise, …) and then post-processing of the most interesting components. This whole series of processing cannot be easily and rapidly done in the field (> 20 min) compared to a simple DStretch® visualization. The data recording is therefore partly blind to the potential presence of "invisible" paintings in the scene. However, automatization of a pipeline including most of the process is possible, at least for a given type of measurement, but it still needs to be developed and standardized. Nevertheless, it should be kept in mind that the amount of information contained in a single data cube is very large (300 Mo to 50 Go) and its complete exploitation, beyond the simple separation of pigments, may need additional analyses and tools. For example, an extension of the processing may consist in performing local analyses of the images, focusing on local variations of pigments and rock texture in and around a single figure. If the subset selection reduces the variability in the image part under study, it may help to discover small additional figures or details which were otherwise buried in the noise. In a second stage, the use of well-adapted hyperspectral pixel classification tools and techniques may allow a sharper separation of the different types of pigments and their projection on high spatial resolution camera image [70], with their 'original' color rendering, thanks to the conversion of their visible reflectance spectrum into photometric information.

However, a small software running a pre-optimized ICA transformation on HSI data complemented with some simple visualization functions should be as easy to manage as with DStretch® on RGB camera images and will provide much better results due to the better separation between the various pigment and rock contributions and the removal of a large part of the high spatial instrument and natural noises.

Data reduction steps of HSI image may be even easier and more reproducible as only global and standard image processing functions may be used thanks to the better separation of information by ICA. For example, a simple global thresholding of some of the ICA components (i.e. a black and white image) can already provide a quite clean distribution map for some pigments, without having to use sophisticated functions and local manipulation to extract the pixels of a figure in image processing software.

Conclusions

The "HSI revolution" that has emerged from space exploration and now back on Earth may provide archaeologists with a new way to access more information than in the past while respecting the integrity of rock paintings. It is a new step in the evolution of the methods for documentation of rock art. It is advisable to recall nevertheless that it does not eliminate the subjectivity of the survey, since, whatever the chosen mode of operation, the human intervention is always preponderant at the acquisition step, but also at the analysis and interpretation steps [2, 71]. Nevertheless, HSI instruments made it possible to push back the limits of the standard RGB cameras.

An RGB camera image of Neolithic painting on oxidized sandstone analyzed with DStretch® can be sufficient to visualize part of the figures, generally the most recent, or even all the figures in the scene when they have sufficient color contrasts between them and with the rock. Now, with a hyperspectral data cube recorded with a VNIR HSI instrument we can better remove the wall texture as well as the natural noise and extract the distribution of the various pigments with a greater contrast. When the color contrast of a figure with the surrounding rock, or figures, becomes poor or statistically null, due to the progressive alteration of both paint and rock, an HSI can reveal new figures by capitalizing both on its strong ability to extract the distribution of the different pigment types, and on the new discriminating information contained in the very near infrared part of the spectrum. Another important result is that measurement of shaded walls is not a major problem, mostly slightly reducing the VNIR spectral range and increasing measurement time,

but possibly positively reducing the natural high spatial frequency noise linked to rock and pigment microtextures that otherwise strongly disturb the extraction of pigmented pixels.

HSI measurements are especially useful when the figures have a complex organization in the scene with numerous juxtapositions or layer superimpositions, when they are polychromatic, and when in addition some of them are very faint. In that case a dozen information components are needed to describe correctly the variety of pigment and rock composition, texture and alteration degrees. In such a case, quite frequent indeed, a few dozen well distributed spectral channels are a minimum to sample all this information as well as the different sources and pattern of noises, to best remove them. Thus, from this point of view, one can easily realize that an RGB camera can only record highly degraded information with its only three wide spectral filters covering a limited spectral range, a strong physical limitation that DStretch® cannot improve in any way. Our eye, with a similar color information collection process, is well known to have a sensitivity covering less than an octave (a factor of 2) and to be a poor discriminator of wavelength [72]. It is thus absolutely unable to recognize the individual wavelengths of two combined monochromatic sources, contrary to our ear that can recognize the combination of 2 or more tones over at least 5–6 octaves. It is what a VNIR HSI instrument can do over about 1.5 octaves and almost 3 octaves for a coupled VNIR-SWIR instrument.

With a VNIR instrument only, even able to record larger images at higher spatial resolution, the capability to go to the next scientific step of the identification and mapping of the composition of pigments is quite limited as mostly the chromophore minerals (hematite, goethite, …) play a role and can be identified in this spectral range. It should be noted here that an RGB + DStretch® image gives no access to such information. A SWIR HSI instrument covering the 1–2.5 µm range is needed to map chemical and mineral composition of pigments and rock. It should also improve the separability of pigments of similar visual color; allow us to group figures on the basis of their composition; and provide clues as to the presence of mineral phases associated with the pigment giving indications on possible intentional mixtures and on the origin of the raw materials. But a SWIR HSI instrument implies a much heavier logistic on the field.

The speed and ease of obtaining powerful and reliable results are essential conditions for documenting rock sites in mountainous or desert areas where access difficulties, extreme environment conditions and field logistics are crucial. For such exploratory campaigns DStretch® allows a quick deciphering of the walls, which facilitates the acquisition of precise and detailed documentation. Complexity is not a guarantee of performance, and for the Saharan terrain, efficiency is the essential quality to privilege. At the moment, RGB cameras with DStretch® is still an unavoidable combination of tools for field research. Its partially automatized decorrelation of image channels specifically dedicated to enhance pigments makes it easy and fast to use and very popular among most rock art recorders [5, 24]. Previous tests of PCA run on RGB images showed that they gave slightly better results (5%) than DStretch, but the difference was not considered enough to revolutionize the field [63]. But a compact and lightweight VNIR HSI (or multispectral) camera should become the best companion of Neolithic painting explorers as we demonstrated that its added archaeological value is very significant.

Currently the three major limitations of HSI cameras, compared to RGB cameras, are first the size of the image, typically an order of magnitude smaller in both directions, which constrains either the size of the figure or panel recorded, and/or the pixel spatial resolution: a strong limitation when there are narrow drawings (sub-mm). And second, the measurement preparation (need to be fixed on a tripod) and recording time (up to 10 min in the worst cases of low light) which limits the number of measurements also by more than an order of magnitude compared to cameras. When the recording time is long there is also the issue of the stability of the illumination, so relatively stable weather conditions are the best, either clear sky or fully cloudy. However, the developments of these types of instruments are fast and image format of portable HSI should steadily increase. There is also a growing number of compact commercial 'snapshot' (or quasi-snapshot) acquisition solutions, with 8 to up to a hundred spectral channels, but generally still with a small image format and sometimes with too large minimum focusing distances for archaeological use (currently mostly developed for UAV). They should in the future reduce the preparation and acquisition time of hyperspectral measurements close to that of a normal camera. When these instruments will be mature and will have overcome some of their restrictive characteristics, they will be the perfect and powerful camera in remote area.

The last limitation is the data processing, as ICA is a time-consuming convergence algorithm and involves also a visual selection of the relevant components, which may be more than 3, to be displayed in B&W or RGB. Currently, unlike DStretch®, this processing cannot be performed on site, but the development of dedicated plugins can be considered.

However, back from the field, data analysis with ICA can be efficiently computed with dedicated software (such as ENVI) on powerful computers. It requires a little

bit more skills to preselect the best wavelength range and some ICA parameters, but some of these steps may be automatized to get the best results for rock art. With the coupled use of hyperspectral images and ICA algorithms the gains in detectivity and separability between pigments and with rock wall texture is such that it should make the extraction of faint or barely-visible painting easier, faster and more reproducible than with camera, even with the current limitations of the instruments.

In the following, we suggest a photographic strategy for remote and hard-to-reach area in 3 steps:

Step 1: Identify the paintings

- Use of RGB cameras (e.g. last generation smartphone cameras) with onboard DStretch® or similar software to (1) help rapidly explore shelters, especially those hard-to-reach, (2) visualize on-site the faint paintings to assess their potential interest, and (3) systematically record the figures, their locations and extend, or tracks of pigments on the wall.
- Use a lightweight VNIR HSI camera to record the most complex panels, in terms of polychromies, figure superposition, or variability / complexity of rock texture and color of the wall. Also make some global low-resolution measurements on potential panels where no clear figure is visible either by eye or on DStretched images.
- Possibly use lightweight and foldable sun reflectors directed toward the shaded panel to increase the spectral range up to 1000 nm (but may induce illumination inhomogeneities).

Step 2: Systematic recording of the paintings of whole panels

- Use of a high performance VNIR HSI instrument (1500–3000 pixels swath) to easily cover large scenes at high spatial resolution
- Use lighting lamps for shaded walls (but energy consuming) to reduce acquisition time and benefit from the full very near infrared range, up to 1000 nm.
- Complement measurements with a portable VNIR-SWIR point spectrometer to record typical and end-member spectra of paint and rock wall over the full spectral range (but may need on-site HSI data preprocessing to locate them accurately) for pigment and rock composition determination.

Step 3: Mapping of the pigment composition and rock taphonomy

- In addition, use a SWIR HSI instrument (1000–2500 nm) to improve the pigment separability and map pigment composition and rock taphonomy (mineral identification). But these measurements in the near-infrared will be only possible in sunlight (but restricted outside the strong atmospheric water bands), or better, with a powerful artificial halogen lighting to cover the whole spectral range (further increasing weight, complexity and power consumption). This step can be also complemented with 3D acquisition with digital photogrammetry and three-dimensional scanner laser [73, 74].

In order to be efficient in the field for the exploratory phase (step 1) it should be useful to get on-site a first guess of the interest of HSI measurements of some area. So, a fast and automatic data analysis pipeline run just after recording should be developed to assess if more extended data cube measurements or at higher spatial resolution are needed.

Also, in this exploratory study we only analyzed the main 'paint' components of the ICA transformation as well as comparisons between some end-member spectra of the major ICA components of interest. We have shown only one example, in a simple case (panel #1), of complete pigment extraction and overlay on the original image after 'restoration' of the color with a higher contrast with the rock. However, various other post-processing operations may be performed on the hyperspectral data and their analysis products depending of the final goal (figures and scene reconstruction, chronological study, pigment composition, …).

Many different tools have been developed, in addition to the mathematical transformations used here, to help distinguish between the different pigments and classify them in a series of homogeneous classes for further analysis in terms of color, composition, painting technique, superposition, etc. After the spectral concentration of information performed by the ICA, this step corresponds to the spatial dimension reduction and concentration of the information [75]. These tools can work either directly on the original hyperspectral data cube, or on a selected set of ICA, PCA or MNF components, or even on denoised hyperspectral data cubes reconstructed by filtering out the noise components followed by an inverse transformation [66]. These tools, once adapted to the data and the specific problem to be solved, have proven over the last three decades to be very useful and efficient in many fields of remote sensing (e.g. planetary sciences or Earth monitoring) as well as in painting arts of all ages.

Regarding rock arts, they need to be tested and adapted to the types of pigment and rock wall color, composition, texture and alteration types. But also, to fieldwork and its specific lighting conditions. The case treated in this exploratory article of red–orange pigments painted on

oxidized sandstone walls and subjected to strong corrasion was a good example and a rather difficult case to test the technique. But it proved the great potential of VNIR HSI instruments to uncover new figures hidden to the naked eye and to effectively separate their pigments from the wall substrate. We believe that these instruments open up new and exciting horizons for the study of rock and cave paintings.

Acknowledgements
Not applicable.

Author contributions
BS and F-VD made the hyperspectral measurements, wrote the main manuscript text and prepared figures. F-VD and FD made the camera measurements and DStretch treatments. BS made the hyperspectral analysis. All authors contributed to the interpretation, read and approved the manuscript. All authors read and approved the final manuscript.

Funding
The authors did not receive support from any organization for the submitted work.

Availability of data and materials
The full datasets recorded and analyzed during the current study are available from the corresponding author on reasonable request. A set of the data will be available in a free repository.

Declarations

Competing interests
The authors declare that they have no competing interests.

Received: 26 December 2022 Accepted: 23 April 2023
Published online: 08 May 2023

References

1. Duquesnoy F. Apport des outils numériques et informatiques à l'étude des images rupestres du Sahara central : exemple d'application aux peintures de Séfar (Tasïli-n-Ăjjer, Algérie) (Doctoral dissertation, Aix-Marseille) 2015.
2. Brady LM. Documenting and analyzing rock, paintings from Torres Strait, NE Australia, with digital photography and computer image enhancement. J Field Archaeol. 2006;31:363–79.
3. McNiven IJ, David B, Brady L, Brayer J. Kula Rock-Art Site, Dauan Island, Torres Strait. Mem Queensl Mus Cult. 2004;3:227–55.
4. Fritz C, Tosello G. The hidden meaning of forms: methods of recording Paleolithic parietal art. J Archaeol Method and Theory. 2007;14:48–80.
5. Brady L, Hampton J, Domingo Sanz I. Recording rock art: strategies, challenges, and embracing the digital revolution. In: David B, McNiven I, editors. The Oxford handbook of the archaeology and anthropology of rock art. Oxford: Oxford Academic; 2017. https://doi.org/10.1093/oxfordhb/9780190607357.013.37.
6. Montero Ruiz I, Rodríguez Alcalde ÁL, Vicent García JM, Cruz BM. Técnicas digitales para la elaboración de calcos de arte rupestre. Trab Prehist. 1998;55:155–69.
7. David B, Brayer J, McNiven IJ, Watchman A. Why digital enhancement of rock paintings works: rescaling and saturating colours. Antiquity. 2001;2001(75):781–92.
8. Rogerio-Candelera MA, Vanhaecke F, Resano M, Marzo P, Porca E, Alloza R, Sáiz-Jiménez C. Combinación de análisis de imagen y técnicas analíticas para la distinción de diferentes fases en un panel rupestre (La Coquinera II, Obón, Teruel) 2009.
9. Gunn RG, Ogleby CL, Lee D, Whear RL. A method to visually rationalise superimposed pigment motifs. Rock Art Res J Aust Rock Art Res Assoc. 2010;27:131–6.
10. Brady LM, Gunn RG. Digital enhancement of deteriorated and superimposed pigment art: methods and case studies. In: McDonald J, Veth P, editors. A companion to rock art, Chap. 35. Hoboken: Blackwell Publishing Ltd; 2012. p. 627.
11. Duquesnoy F, Souidi Z, Donzé FV. The forgotten rock paintings of the wadi Ġerat. Cahiers de l'AARS—N. 2020;21:33–48.
12. Rip MR. Digital recording and image processing of rock art by computer. South Afr Archaeol Bull. 1983;38:77–9.
13. Rip MR. Colour space transformations for the enhancement of rock art images by computer. Rock Art Res. 1989;6:12–6.
14. De Cola L. Pulizia elettronica (pe) di dipinti e graffiti rupestri: Un rilievo tratto da immagini elaborate presentate ad Arles (1994). In : Actes de l'assemblée annuelle de l'Association des amis de l'art rupestre saharien (Turin, 28–29 août 1995; Ingolstadt, 17–18 mai 1996) 1997. pp. 19–21.
15. Arcà A. Digital auto-tracing in rock art recording. Applications of computer vectorial design. TRACCE Online Rock Art Bull 11. 1999; http://www.rupestre.net/tracce/?p=1989. Accessed 13 July 2022.
16. Donnan EF. Recording British rock art, TRACCE Online Rock Art Bull 11. 1999; http://www.rupestre.net/tracce/?p=2024. Accessed 13 July 2022.
17. Clogg P, Díaz-Andreu M, Larkman B. Digital image processing and the recording of rock art. J Archaeol Sci. 2000;27:837–43.
18. Rogerio-Candelera MA, Jurado V, Laiz L, Sáiz-Jiménez C. Laboratory and in situ assays of digital image analysis based protocols for biodeteriorated rock and mural paintings recording. J Archaeol Sci. 2011;38:2571–8.
19. Donzé FV, Souidi Z, Donzé-Magnier M, Magnier SA. Evolution of the preservation state of cave paintings in Wadi in Djaren, Southern Tadrart, Algeria, Geonum Ed.: ISRN GEONUM-NST--2018–03—EN, 2018.
20. Sanz ID, Montalvo EL. Metodología: el proceso de obtención de calcos o reproducciones. In: La Cova dels Cavalls en el Barranc de la Valltorta. Museu de la Valltorta (Tirig). 2002; pp. 75–81.
21. Mark R, Billo E. Computer-assisted photographic documentation of rock art. Coalit CSIC Themat Netw Cult Herit. 2006;11:10–4.
22. Brady LM. A different look: Comparative rock-art recording from the Torres Strait using computer enhancement techniques. Aust Aborig Stud. 2007;1:98–115.
23. Harman J. Using decorrelation stretch to enhance rock art images. In: American Rock Art Research Association Annual Meeting (Vol. 28). 2005. http://www.dstretch.com/AlgorithmDescription.pdf. Accessed 31 Oct 2021.
24. Le Quellec JL, Duquesnoy F, Defrasne C. Digital image enhancement with DStretch: is complexity always necessary for efficiency? Digit Appl Archaeol Cult Herit. 2015;2:55–67.
25. Fraile FJL, Garcia LMG, Klink AC. 3D documentation and use of DStretch for two new sites with post-paleolithic rock art in Sierra Morena, Spain. Rock Art Res. 2016;33:127–42.
26. Troncoso A, Moya F, Basile M. Rock art and social networks among hunter gatherers of north-central Chile. J Anthropol Archaeol. 2016;42:154–68.
27. Quesada E, Harman J. A step further in rock art digital enhancements. DStretch on Gigapixel imaging. Digit Appl Archaeol Cult Herit. 2019;13:e00098.
28. Le Quellec JL, Harman J, Defrasne C, Duquesnoy F. DStretch® et l'amélioration des images numériques: applications à l'archéologie des images rupestres. Cahiers de l'AARS. 2013;16:177–98.
29. Soha JM, Schwartz AA. Multispectral histogram normalization contrast enhancement. In: 5th Canadian Symp Rem Sens. 1979; pp. 86–93.
30. Alley R. Algorithm theoretical basis document for decorrelation stretch, version 2.2, Pasadena, jet propulsion laboratory, AST06 report. 1996; p. 18. https://eospso.gsfc.nasa.gov/sites/default/files/atbd/ASTER_ATBD_99-2010.pdf. Accessed Oct 2020.
31. Jiang J, Liu D, Gu J, Süsstrunk S. What is the space of spectral sensitivity functions for digital color cameras?. WACV 2013. http://www.gujinwei.org/research/camspec/camspec.pdf. Accessed 12 Sept 2022.
32. Sharpe LT, Stockman A, Jagla W, Jägle H. A luminous efficiency function, V*(λ), for daylight adaptation. J Vis. 2005;5:948–68.

33. Borengasser M, Hungate WS, Watkins R. Hyperspectral remote sensing: principles and applications. Boca Raton: CRC Press, Taylor & Francis Series in Remote Sensing Applications; 2007.
34. Aiazzi B, Alparone L, Baronti S, Lastri C, Selva M. Spectral distortion in lossy compression of hyperspectral data. J Electr Comput Eng. 2012. https://doi.org/10.1155/2012/850637.
35. Rocard F, Barat C, Bertaux JL, Bibring JP, Blamont JE, Bonneau F, et al. French participation in the Soviet Phobos mission. Acta Astronaut. 1990;22:261–7.
36. Goetz AFH, Vane G, Solomon JE, Rock BN. Imaging spectrometry for earth remote sensing. Science. 1985;228:1147–53.
37. van der Meer FD, van der Werff HMA, van Ruitenbeek FJA, Hecker CA, Bakker WH, et al. Multi-and hyperspectral geologic remote sensing: a review. Int J Appl Earth Obs Geoinf. 2012;14:112–28.
38. Khan MJ, Khan HS, Yousaf A, Khurshid K, Abbas A. Modern trends in hyperspectral image analysis: a review. IEEE Access. 2018;6:14118–29.
39. Lu G, Fei B. Medical hyperspectral imaging: a review. J Biomed Opt. 2014;19:010901.
40. Cucci C, Delaney JK, Picollo M. Reflectance hyperspectral imaging for investigation of works of art: old master paintings and illuminated manuscripts. Acc Chem Res. 2016;49:2070–9.
41. Laureti S, Malekmohammadi H, Rizwan MK, Burrascano P, Sfarra S, Mostacci M, Ricci M. Looking through paintings by combining hyper-spectral imaging and pulse-compression thermography. Sensors. 2019;19:4335.
42. Pronti L, Romani M, Verona-Rinati G, Tarquini O, Colao F, Colapietro M, Pifferi A, Cestelli-Guidi M, Marinelli M. Post-processing of VIS, NIR, and SWIR multispectral images of paintings. New discovery on the *The Drunkenness of Noah,* painted by Andrea Sacchi, stored at Palazzo Chigi (Ariccia, Rome). Heritage. 2019;2(3):2275–86.
43. Cucci C, Picollo M, Chiarantini L, Uda G, Fiori L, De Nigris B, Osanna M. Remote-sensing hyperspectral imaging for applications in archaeological areas: non-invasive investigations on wall paintings and on mural inscriptions in the Pompeii site. Microchem J. 2020;158:105082.
44. Li GH, Chen Y, Sun XJ, Duan PQ, Lei Y, Zhang LF. An automatic hyperspectral scanning system for the technical investigations of Chinese scroll paintings. Microchem J. 2020;155:104699.
45. Alfeld M, de Viguerie L. Recent developments in spectroscopic imaging techniques for historical —a review. Spectrochim Acta B. 2017;136:81–105.
46. Daveri A, Paziani S, Marmion M, Harju H, Vidman A. New perspectives in the non-invasive, in situ identification of painting materials: the advanced MWIR hyperspectral imaging. Trends Anal Chem. 2018;98:143–8.
47. Polaka A, et al. Hyperspectral imaging combined with data classification techniques as an aid for artwork authentication. J Cult Herit. 2017;26:1–11.
48. Peeters J, Van der Snickt G, Sfarra S, Legrand S, Ibarra-Castanedo C, Janssens K, Steenackers G. IR reflectography and active thermography on artworks: the added value of the 1.5–3 µm band. Appl Sci. 2018;8:50.
49. Laureti S, Colantonio C, Burrascano P, Melis M, Calabrò G, Malekmohammadi H, Sfarra S, Ricci M, Pelosi C. Development of integrated innovative techniques for paintings examination: the case studies of The Resurrection of Christ attributed to Andrea Mantegna and the Crucifixion of Viterbo attributed to Michelangelo's workshop. J Cult Herit. 2019;40:1–16.
50. Chalmin E, Schmitt B, Chanteraud C, de Kergommeaux AC, Soufi F, Salomon H. How to distinguish red coloring matter used in prehistoric time? The contribution of visible near-infrared diffuse reflectance spectroscopy. Color Res Appl. 2021;46:653–73.
51. Romani M, Capobianco G, Pronti L, et al. Analytical chemistry approach in cultural heritage: the case of Vincenzo Pasqualoni's wall paintings in S. Nicola in Carcere (Rome). Microchem J. 2020;156:104920.
52. Vicent JM, Montero I, Rodríguez A, Martínez I, Chapa T. The use of multiband imaging for the study and preservation of post-paleolithic rock art. Trab de Prehist. 1996;53:19–35.
53. Robinson EJ, Ware GA. Multi-spectral imaging of La Casa de las Golondrinas rock paintings. 2002. http://www.famsi.org/reports/99052/99052Robinson01.pdf. Accessed 07 Feb 2023.
54. Hain M, Bartl J, Jacko V. Multispectral analysis of cultural heritage artefacts. Meas Sci Rev. 2003;3:9–12.
55. Skoog B, Helmholz P, Belton D. Multispectral analysis of indigenous rock art using terrestrial laser scanning. The International Archives of the Photogrammetry, Remote Sensing and Spatial Information Sciences, Volume XLI-B5, 2016 XXIII ISPRS Congress, 12–19 July 2016, Prague, Czech Republic. pp. 405–12
56. Bayarri Cayón V. Algoritmos de análisis de imágenes multiespectrales e hiperespectrales para la documentación e interpretación del arte rupestre. Universidad Nacional de Educación a Distancia (España). Escuela Internacional de Doctorado. Programa de Doctorado en Tecnologías Industriales. 2020.
57. Bayarri V, Latova J, Castillo E, Lasheras JA, De Las Heras C, Prada A. Nueva documentación y estudio del arte empleando técnicas hiperespectrales en la Cueva de Altamira. In XIX International Rock Art Conference IFRAO 2015. Symbols in the Landscape: Rock Art and its Context. Conference Proceedings; Instituto Terra e Memória: Tomar, Portugal, 2015; ISBN 978-84-9852-463-5.
58. Ripoll S, Bayarri V, Castilloz, E, Latova J, Munoz F. El Panel de las Manos de la Cueva de El Castillo (Puente Viesgo, Cantabria). ARKEOS|perspectivas em diálogo, nº 37. In XIX International Rock Art Conference IFRAO 2015. Symbols in the Landscape: Rock Art and its Context. Conference Proceedings; Instituto Terra e Memória: Tomar, Portugal, 2015; ISBN 978-84-9852-463-5.
59. Bayarri V, Sebastián MA, Ripoll S. Hyperspectral imaging techniques for the study, conservation and management of rock art. Appl Sci. 2019;9:5011.
60. Bayarri V, Castillo E, Ripoll S, Sebastián MA. Improved application of hyperspectral analysis to rock art panels from El Castillo cave (Spain). Appl Sci. 2021;11:1292.
61. Cook KH, Vizy EK. Detection and analysis of an amplified warming of the Sahara Desert. J Climate. 2015;28:6560–80.
62. Faci M, Oubadi M, Matari A, Farhi Y. Heat waves in Algeria: a potential risk. Int J Innov Tech Appl Sci. 2018;2:13–21.
63. Domingo I, Carrión B, Blanco S, Lerma JL. Evaluating conventional and advanced visible image enhancement solutions to produce digital tracings at el Carche rock art shelter. Digit Appl Archaeol Cult Herit. 2015;2:79–88.
64. Behmann J, Acebron K, Emin D, Bennertz S, Matsubara S, Thomas S, et al. Specim IQ: evaluation of a new, miniaturized handheld hyperspectral camera and its application for plant phenotyping and disease detection. Sensors. 2018;18:441.
65. Hyvarinen A, Oja E. Independent component analysis: algorithms and applications. Neural Netw. 2000;13:411–30.
66. Schmitt B, Philippe S, Grundy WM, Reuter DC, Côte R, Quirico E, et al. Physical state and distribution of materials at the surface of Pluto from New Horizons LEISA imaging spectrometer. Icarus. 2017;287:229–60.
67. Rogerio-Candelera MÁ. Digital image analysis based study, recording, and protection of painted rock art. Some Iberian experiences. Digit Appl Archaeol Cult Herit. 2015;2:68–78.
68. Ontañó R, Bayarri V, Castillo E, Montes R, Morlote JM, Muñoz E, Palacio E. New discoveries of pre-Magdalenian cave art in the central area of the Cantabrian region (Spain). J Archaeol Sci Rep. 2019;28:102020.
69. Cerrillo-Cuenca E, Sepúlveda M, Guerrero-Bueno Z. Independent component analysis (ICA): a statistical approach to the analysis of superimposed rock paintings. J Archaeol Sci. 2021;125:105269.
70. Defrasne C, Massé M, Giraud M, Schmitt B, Fligiel D, Le Mouélic S, Chalmin E. The contribution of VNIR and SWIR hyperspectral imaging to rock art studies: example of the Otello schematic rock art site (Saint-Rémy-de-Provence, Bouches-du-Rhône, France. Archaeol Anthropol Sci. 2022. https://doi.org/10.21203/rs.3.rs-2250615/v1.
71. Read EJ, Chippindale C. Electronic drawing or manual drawing? Experiences from work with rock-paintings. BAR Int Ser. 2000;844:59–80.
72. Wyszecki G, Stiles WS. Color science: concepts and methods, quantitative data and formulae. 2nd ed. New York: Wiley; 1982.
73. Domingo I, Villaverde V, López-Montalvo E, Lerma JL, Cabrelles M. Latest developments in rock art recording: towards an integral documentation of Levantine rock art sites combining 2D and 3D recording techniques. JAS. 2013;40:1879–89.
74. Jalandoni A. An overview of remote sensing deliverables for rock art research. Quatern Int. 2021;572:131–8.
75. Dabiri Z, Lang S. Comparison of independent component analysis, principal component analysis, and minimum noise fraction transformation for tree species classification using APEX hyperspectral imagery. ISPRS Int J Geo Info. 2018;7:488.

Publisher's Note